Departament de Teoria
del Senyal i Comunicacions
UNIVERSITAT POLITÈCNICA DE CATALUNYA

MULTIDIMENSIONAL SPECKLE NOISE, MODELLING AND FILTERING RELATED TO SAR DATA

by

Carlos López Martínez

Xavier Fàbregas Cànovas, Thesis Advisor

Ph.D. Dissertation

Thesis Committee: Antoni Broquetas i Ibars
Ignasi Corbella i Sanahuja
Jong-Sen Lee
Eric Pottier
Juan Manuel López Sánchez

Barcelona, June 2, 2003

Chapter 5

Multidimensional Speckle Noise Model

5.1 Introduction

As it was pointed out at Chapter 2, multidimensional SAR systems are important as they offer the possibility to enhance the capability to analyze the scatterer's properties via multiple system geometries, polarizations or frequencies. In the case of point scatterers, the significant information can be accurately recovered. On the contrary, for distributed scatterers this is not the case as a result of speckle noise. Such a targets are objects of interest in many applications, among which one can underline: agriculture, forestry or hydrology. Consequently, a primary step in extracting information from distributed scatterers is to understand how speckle noise corrupts this information.

The study of speckle noise orbits around zero-mean, complex Gaussian processes. When these processes are considered separately, useful information can only be obtained from intensity data. On the contrary, for correlated processes, the coherent combination of data has been proved to be an important source of information about the scatterer. On the basis of the moment theorem for complex gaussian processes [111, 110, 179], one can see that second moments are the cornerstone from an information content point of view. Consequently, the complex Hermitian product of a pair of SAR images is the key information source. But, despite a speckle noise model exist for one-dimensional SAR imagery, it does not exist for multidimensional SAR imagery [7, 1, 167].

Most of the times, the multidimensional speckle noise problem has been addressed from a polarimetric point of view in the literature, and always with the objective to reduce it. Some examples can be found in [37,39,40,1]. Nevertheless, the multidimensional speckle problem is also present in dimensionally higher problems as Polarimetric SAR Interferometry (PolInSAR) [180] or even in multi frequency systems [181]. The core of this chapter concerns the proposal of a new polarimetric speckle noise model for SAR data [182, 183], based on the theory introduced within the last chapter. Additionally, it will be shown that the proposed model is in accordance with all the previous theory about speckle. On the other hand, the polarimetric speckle model will be shown to be also valid for PolInSAR and multifrequency systems. Finally, a multidimensional SAR speckle noise model will be proposed.

5.2 Preliminaries

The process, which will finish with a multidimensional speckle noise model, is based on a constructive approach. In brief, the ideas introduced in Section 4.2, within Chapter 4, for the phase difference phasor represent here the basis for the multidimensional speckle noise model. Amplitude information is combined

with the unit amplitude phasor model in order to arrive to a speckle noise model for the Hermitian product of a pair of SAR images. Finally, the multidimensional speckle noise model is straightforwardly obtained from the complex Hermitian product speckle noise model.

The Hermitian product of a pair of SAR images is a key quantity since it represents the basic building block when multidimensional SAR imagery is addressed. In the case of PolSAR, this product represents the basis for the construction of the covariance and coherency matrices [77]. Additionally, its argument provides the phase difference, which has been shown to contain relevant information about the scatterer [91, 20]. PolSAR data is the ideal vehicle to introduce a multidimensional speckle noise model, as well as a way to study its implications. In the following, the multidimensional speckle noise model will be established over the covariance matrix, which has been introduced in Section 2.3.4 on page 44.

The importance of the Hermitian products also emerges from a statistical point of view. As introduced at Chapter 2, SAR images can be assumed to be described by zero-mean, complex Gaussian probability density functions (pdf), represented by $\mathcal{N}_c(0, \sigma^2/2)$, whereas correlated SAR images can be acquired varying one, or several imaging parameters. Let $\mathbf{k} = [S_1, S_2, \ldots, S_Q]^T$ be a set of Q correlated SAR images distributed as $\mathcal{N}(\mathbf{0}, [C])$. By the moment theorem for complex Gaussian processes [111, 110, 179]:

(a) If $k \neq l$, then

$$E\{S_{m_1} S_{m_2} \cdots S_{m_k} S^*_{n_1} S^*_{n_2} \cdots S^*_{n_l}\} = 0 \tag{5.1}$$

where m_k and n_l are integers from the set $\{1, 2, \ldots, Q\}$.

(b) If $k = l$, then

$$E\{S_{m_1} S_{m_2} \cdots S_{m_k} S^*_{n_1} S^*_{n_2} \cdots S^*_{n_l}\} = \sum_{\pi} E\{S_{m_{\pi(1)}} S^*_{n_1}\} E\{S_{m_{\pi(2)}} S^*_{n_2}\} \cdots E\{S_{m_{\pi(l)}} S^*_{n_l}\} \tag{5.2}$$

where π is a permutation of the set of integers $\{1, 2, \ldots, l\}$.

Consequently, the complex SAR images S_q cannot be independently averaged, since as demonstrated, are zero mean. The second point, Eq. (5.2), establishes that useful information is contained within even moments. But, as it can be observed, even moments of order higher than two can be directly obtained as a combination of second moments. As a result, it is only necessary to study the effects of speckle noise over the Hermitian product of a pair of SAR images, since higher moments result from the combination of them.

The properties of the Hermitian product of a pair of SAR images can be completely determined under a 2 by 2 covariance matrix formulation. This approach is widely employed in the related literature [21, 22] and has been already introduced in Section 2.2.3 to analyze the interferometric phase statistics. Let S_1 and S_2 be a pair of SAR images described by zero-mean, complex Gaussian pdfs. At is has been defined at Sections 2.2.3 and 2.3.3, the scatterer vector $\mathbf{k}$, constructed as $\mathbf{k} = [S_1 \;\; S_2]^T$, is described by the pdf $\mathcal{N}(\mathbf{0}, [C])$

$$p_{\mathbf{k}}(\mathbf{k}) = \frac{1}{\pi^2 |[C]|} \exp(-\mathbf{k}^{*T} [C]^{-1} \mathbf{k}) \tag{5.3}$$

where $[C]$ denotes the covariance matrix which contains the SAR images correlation structure. $|[C]|$ represents the covariance matrix determinant. The covariance matrix can be represented in this case as

$$[C] = E\{\mathbf{k}\mathbf{k}^{*T}\} = \begin{bmatrix} \sigma_1 & \psi\rho \\ \psi\rho^* & \sigma_2 \end{bmatrix} \tag{5.4}$$

where ^{*T} indicates transpose complex conjugate. The parameters σ_1 and σ_2 represent the backscattering coefficient of the SAR images S_1 and S_2 respectively, being defined as $\sigma_k = E\{|S_k|^2\}_{k\in\{1,2\}}$. ψ is a measure of the average power in the two channels

$$\psi = \sqrt{\sigma_1 \sigma_2}. \tag{5.5}$$

The symbol ρ, as is has been defined at Chapter 2, represents the complex correlation coefficient between a pair of SAR images, defined as

$$\rho = |\rho| \exp(j\phi_x) = \frac{E\{S_1 S_2^*\}}{\sqrt{E\{|S_1|^2\}E\{|S_2|^2\}}}. \tag{5.6}$$

By convention, its amplitude $|\rho|$ is called simply coherence, whereas the phase ϕ_x contains the effective phase difference between the pair of SAR images.

Given the pair of SAR images S_1 and S_2, the single-look (or sample) covariance matrix $[Z]$ is defined as

$$[Z] = \begin{bmatrix} S_1 S_1^* & S_1 S_2^* \\ S_2 S_1^* & S_2 S_2^* \end{bmatrix}. \tag{5.7}$$

As introduced at Section 2.3.5, since the target vector $\mathbf{k}$ is described as $\mathcal{N}(\mathbf{0}, [C])$, the single-look covariance matrix, Eq. (5.7), is described by a complex Wishart distribution $\mathcal{W}([C], 1)$, whose expression has been already introduced at Section 2.3.5, Eq. (2.181), with $[C]$ defined as given by Eq. (5.4). Eqs. (5.1) and (5.2) state the importance of the Hermitian product, from a statistical point of view, for multidimensional SAR imagery, since they are the entries of the single-look covariance matrix $[Z]$, from which the matrix $[C]$ has to be estimated. Recent advances in statistical analysis have made possible to find a closed expression for the kth moments of the matrix $[Z]$, understood as $E\{[Z]^k\}$, showing that all moments of $[Z]$ are function of $[C]$. This fact confirms, on the one hand, that a correct estimation of the covariance matrix $[C]$ is the sufficient statistics to characterize SAR imagery under the Gaussian scattering assumption, and, on the other hand, the importance of the Hermitian product of a pair of SAR images as a basic information unit.

Complex SAR images can be represented as $S_k = r_k \exp(\theta_k)$. Hence, a transformation of variables allows to derive the joint pdf of the amplitudes r_1 and r_2 and the phases θ_1 and θ_2 from $\mathcal{W}([C], 1)$ as

$$p_{r_1,r_2,\theta_1,\theta_2}(r_1, r_2, \theta_1, \theta_2) = \frac{r_1 r_2}{\pi^2 \psi^2 (1 - |\rho|^2)} \exp\left(-\frac{\sigma_2 r_1^2 + \sigma_1 r_2^2 - 2\psi|\rho| r_1 r_2 \cos(\theta_1 - \theta_2 - \phi_x)}{\psi^2(1 - |\rho|^2)} \right). \tag{5.8}$$

Let $z = r_1 r_2$ and $\phi = \theta_1 - \theta_2$ be the amplitude and phase of the Hermitian product of a pair of SAR images, respectively. The corresponding joint pdf can be obtained by introducing these changes of variables in Eq. (5.8), thus

$$p_{z,\phi}(z, \phi) = \frac{2z}{\pi\psi^2(1 - |\rho|^2)} \exp\left(\frac{2|\rho| z \cos(\phi - \phi_x)}{\psi(1 - |\rho|^2)} \right) K_0\left(\frac{2z}{\psi(1 - |\rho|^2)} \right) \tag{5.9}$$

where $K_0(\cdot)$ is the modified Bessel function of third kind. As it can be observed in Eq. (5.9) the amplitude z and the phase ϕ are not statistically independent. Consequently, the amplitude and the phase of the Hermitian product cannot be processed independently. The Hermitian product amplitude pdf can be derived integrating Eq. (5.9) over the variable ϕ

$$p_z(z) = \frac{4z}{\psi^2(1 - |\rho|^2)} I_0\left(\frac{2|\rho| z}{\psi(1 - |\rho|^2)} \right) K_0\left(\frac{2z}{\psi(1 - |\rho|^2)} \right) \tag{5.10}$$

where I_0 is the modified Bessel functions of first kind. The first and second moments of the Hermitian product amplitude are

$$E\{z\} = \psi \frac{\pi}{4} {}_2F_1\left(-\frac{1}{2}, -\frac{1}{2}; 1; |\rho|^2 \right) \tag{5.11}$$

$$E\{z^2\} = \psi^2 (1 + |\rho|^2) \tag{5.12}$$

where ${}_2F_1(a, b; c; z)$ represents the Gauss hypergeometric function. In the same way, the phase pdf can be derived from Eq. (5.9) by integrating over z

$$p_\phi(\phi) = \frac{(1 - |\rho|^2)}{2\pi} \left(\frac{\beta(\frac{1}{2}\pi + \arcsin(\beta))}{(1 - \beta^2)^{3/2}} + \frac{1}{1 - \beta^2} \right) \tag{5.13}$$

where $\beta = |\rho|\cos(\phi - \phi_x)$. The phase's first and second moments have been presented in Section 2.2.3.

Any element of the single-look covariance matrix $[Z]$, Eq. (5.7), can be expressed as follows

$$S_k S_l^* = |S_k S_l^*| e^{j(\theta_k - \theta_l)} = z e^{j\phi} \tag{5.14}$$

whose amplitude z and phase ϕ are distributed as given by Eqs. (5.10) and (5.13), respectively.

Next sections are devoted to present an in-depth study of the Hermitian product $S_k S_l^*$, under a polarimetric point of view, with the objective to identify which are the speckle noise components and to study how they affect the useful information content, which corresponds to the mean value of the Hermitian product.

5.3 Phase Difference Phasor Noise Model

The first part of the preceding chapter concerned the definition of a noise model for the interferometric phasor. Indeed, the interferometric phase difference consists in the phase of the Hermitian product of two SAR images acquired from two slightly different positions. As a result, the interferometric phase difference has been shown to contain information from the terrain's topography. In the case of PolSAR data, the Hermitian product phase contains information about the scattering process in the resolution cell. Independently of the type of information contained in the Hermitian product phase, their statistical behaviors are the same, since InSAR and PolSAR data are constructed on the basis of the Hermitian product of a pair of SAR images distributed as $\mathcal{N}(\mathbf{0}, [C])$. This fact allows to extend the results obtained throughout last chapter to PolSAR data. In fact, those results can be generalized to any Hermitian product of a pair of SAR images in which one, or more imaging parameters are different.

As given by Eq. (5.14), any Hermitian product of a pair of SAR images breaks down into an amplitude and a unitary complex phasor. As InSAR and PolSAR phase differences are described by the same pdf, the additive phase noise model in the real plane, Eq. (4.1), is still valid for PolSAR data [184, 20]. Useful information, in both cases, is contained within the true phase difference ϕ_x. Nevertheless, it has to be mentioned, that, despite the equality of the statistical behaviors, the nature of the true phase ϕ_x differs from InSAR to PolSAR data, as it can be seen at Chapter 2. On the one hand, the phase ϕ_x is a deterministic phase containing topographic information in the case of InSAR data, whereas, on the other hand, the phase ϕ_x corresponds to the average phase in the PolSAR data case. The main difference between both of them is, that, the former is wrapped whereas the later is not. Hence, this difference has to be considered whenever the speckle model which will be defined is employed.

The model for the phase difference phasor Eq. (4.30), defined in the frame of InSAR data, can be employed to model phase information for the polarimetric Hermitian product. The final phase difference phasor noise model, Eq. (4.30), is not employed directly. On the contrary, the intermediate results given by Eqs. (4.19) and (4.20) are considered. These equations represent the real and imaginary parts of the unit amplitude phase difference phasor. Consequently, the real and imaginary parts of any element of the polarimetric covariance matrix, following Eq. (5.14), can be written as

$$\Re\{z e^{j\,\phi}\} = N_c\, z\cos(\phi_x) + z\, v_1' \cos(\phi_x) - z\, v_2' \sin(\phi_x) \tag{5.15}$$

$$\Im\{z e^{j\,\phi}\} = N_c\, z\sin(\phi_x) + z\, v_1' \sin(\phi_x) + z\, v_2' \cos(\phi_x) \tag{5.16}$$

The parameters N_c, v_1' and v_2' are generated by the phase difference noise, that is, by the phase difference distribution. The term N_c has emerged in Chapter 4 as an important quantity since it contains basically the same information as the coherence $|\rho|$. This parameter will be shown as crucial to obtain the multidimensional speckle noise model. On the contrary, v_1' and v_2' have been shown to be zero-mean noise terms. Eqs. (5.15) and (5.16) can be expressed under a complex formulation as

$$z e^{j\phi} = [z N_c + (z v_1' + j\, z v_2')] \exp(j\phi_x). \tag{5.17}$$

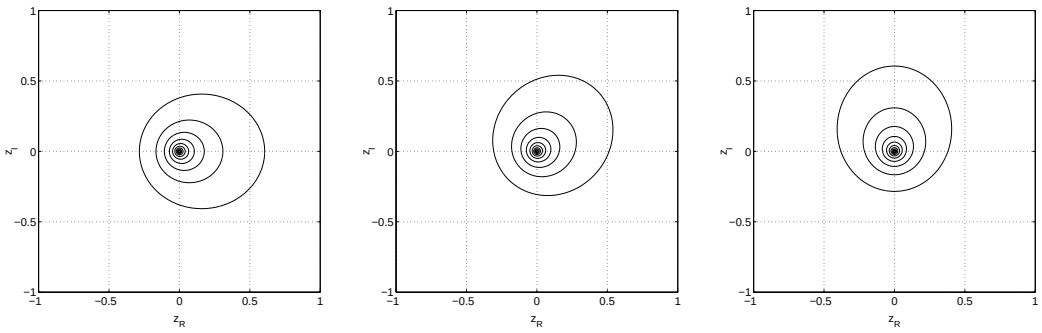

Figure 5.1: Contour plots of the joint pdf $p_{z_R,z_I}(z_R, z_I)$ for the following values of ϕ_x, (a) 0 rad (b) $\pi/4$ rad (c) $\pi/2$ rad and $|\rho| = 0.5$. It can be observed that ϕ_x only introduces a rotation in the complex plane. In all the cases, the maximum is located in the axes origin.

As observed in Eq. (5.17), the true interferometric phasor $\exp(j\phi_x)$ is a multiplicative term within the Hermitian product as a result of the additive phase difference noise model. Consequently, speckle noise will not depend directly on the phasor $\exp(j\phi_x)$. However, it introduces a rotation in the complex plane which will be shown to determine the final nature of the multidimensional speckle noise model in an indirect way.

Eqs. (5.15) and (5.16) give a description for the real and imaginary parts of the Hermitian product of a pair of SAR images expressed as a function of the amplitude z and the phase ϕ_x components. The study of these equations will be based on the amplitude and phase distributions given by Eqs. (5.10) and (5.13) respectively. Nevertheless, it is worth to derive the expressions of the pdfs corresponding to the real and imaginary parts of the Hermitian product. Denoting the Hermitian product real part as $z_R = z\cos(\phi)$ and the imaginary part as $z_I = z\sin(\phi)$, respectively, and introducing these changes of variable into Eq. (5.9), the joint pdf of z_R and z_I is [22]

$$p_{z_R,z_I}(z_R, z_I) = \frac{2}{\pi\psi^2(1-|\rho|^2)} \exp\left(\frac{2|\rho|}{\psi(1-|\rho|^2)}(z_R\cos(\phi_x) + z_I\sin(\phi_x))\right) K_0\left(\frac{2\sqrt{z_R^2+z_I^2}}{\psi(1-|\rho|^2)}\right). \quad (5.18)$$

Fig. 5.1 shows the contour plots of $p_{z_R,z_I}(z_R, z_I)$ for several values of the phase ϕ_x, where the final effect of this parameter can be observed. The marginal pdfs of the Hermitian product real an imaginary parts can be obtained from Eq. (5.18)

$$p_{z_R}(z_R) = \frac{2}{\psi^2(1-|\rho|^2)k_2}\left[\exp(-(k_2-k_1)z_R)H(z_R) + \exp((k_1+k_2)z_R)H(-z_R)\right] \quad z_R \in (-\infty,\infty) \quad (5.19)$$

$$p_{z_I}(z_I) = \frac{2}{\psi^2(1-|\rho|^2)k_2}\left[\exp(-(k_2-k_1)z_I)H(z_I) + \exp((k_1+k_2)z_I)H(-z_I)\right] \quad z_I \in (-\infty,\infty) \quad (5.20)$$

where $H(x)$ represents the Heaviside step function. For $p_{z_R}(z_R)$

$$k_1 = \frac{2|\rho|\cos(\phi_x)}{\psi(1-|\rho|^2)} \quad (5.21)$$

$$k_2 = \frac{2\sqrt{1-|\rho|^2\sin^2(\phi_x)}}{\psi(1-|\rho|^2)}. \quad (5.22)$$

For $p_{z_I}(z_I)$, k_1 and k_2 are obtained by interchanging the terms $\cos(\phi_x)$ and $\sin(\phi_x)$ in Eqs. (5.19) and (5.20). Since for complex, zero-mean Gaussian processes interest lies on their Hermitian products, only the first and second moments for their real and imaginary parts are necessary. For the Hermitian product real part z_R, these are

$$E\{z_R\} = \psi|\rho|\cos(\phi_x) \quad (5.23)$$

$$E\{z_R^2\} = \frac{1}{2}\psi^2[(1-|\rho|^2) + 4|\rho|^2\cos^2(\phi_x)]. \quad (5.24)$$

The moments for the imaginary part z_I are obtained by interchanging the quantities $\cos(\phi_x)$ and $\sin(\phi_x)$ in the previous equations.

5.4 Multidimensional SAR Speckle Noise Model

Introducing the phase difference phasor noise model, Eq. (4.30), one sees that the real and imaginary parts of the Hermitian product of a pair of SAR images break down into three additive terms, see Eq. (5.17). This section concentrates on the analysis of these three terms in order to derive a final speckle noise model for the Hermitian product represented by Eq. (5.14). For simplicity in the following analysis, the three additive terms of Eqs. (5.17) will be referred respectively: the first, the second and the third additive terms. The final objective of this analysis is to find, in each of the three additive terms, noise sources and how them damage the useful information content.

5.4.1 Analysis of $zN_c\exp(j\phi_x)$

The first additive term of Eq. (5.17) refers to the first components of Eqs. (5.15) and (5.16)

$$\Re\{ze^{j\phi}\}_1 = zN_c\cos(\phi_x) \tag{5.25}$$
$$\Im\{ze^{j\phi}\}_1 = zN_c\sin(\phi_x). \tag{5.26}$$

In the following, only Eq. (5.25) will be considered, as the analysis concerning the imaginary part can be obtained straightforwardly by interchanging the $\cos(\phi_x)$ and $\sin(\phi_x)$ terms. Nevertheless, when necessary, expressions for the imaginary part are given. As one sees, these terms depend on the Hermitian product amplitude z, the parameter N_c and the average phase difference. Considering the Hermitian product statistical properties to be homogeneous (i.e., to be constant), the parameter N_c, as well as the phase difference ϕ_x are constant values. As a result, the randomness of the first additive term of the Hermitian product is determined completely by the distribution of the Hermitian product amplitude z, whose distribution is given by Eq. (5.10). If one compares the Hermitian product amplitude mean value, Eq. (5.11), with the mean value of the Hermitian product real part , Eq. (5.23), it can be observed that they present very different values, as expected. For instance, for $|\rho| = 0$, for the normalized power case (i.e., $\psi = 1$), the amplitude mean value equals $\pi/4$ whereas the real part mean value equals 0. This fact makes difficult to base a noise model for the Hermitian product real and imaginary parts directly on the Hermitian product amplitude z.

The first additive noise term of the Hermitian product real part, $\Re\{ze^{j\phi}\}_1$, also depends on the parameter N_c, which has been proved to behave as the coherence $|\rho|$. Regardless of the phase difference dependence, let z_c be a random process defined as

$$z_c = zN_c. \tag{5.27}$$

The pdf of z_c, denoted by $p_{z_c}(z_c)$, is obtained by introducing the change of variable given by Eq. (5.27) into Eq. (5.10). Hence

$$p_{z_c}(z_c) = \frac{4z_c}{\psi^2 N_c^2(1-|\rho|^2)} I_0\left(\frac{2|\rho|z_c}{\psi N_c(1-|\rho|^2)}\right) K_0\left(\frac{2z_c}{\psi N_c(1-|\rho|^2)}\right) \qquad z_c \in [0,\infty). \tag{5.28}$$

Since N_c depends on the coherence $|\rho|$, its effect over $p_z(z)$ is not the one corresponding to a constant value. The limit distributions of $p_{z_c}(z_c)$, as a function of coherence, are

$$\lim_{|\rho|\to 0} p_{z_c}(z_c) = \delta(0) \qquad z_c \in [0,\infty) \tag{5.29}$$
$$\lim_{|\rho|\to 1} p_{z_c}(z_c) = \frac{1}{\psi}e^{-\frac{z_c}{\psi}} \qquad z_c \in [0,\infty). \tag{5.30}$$

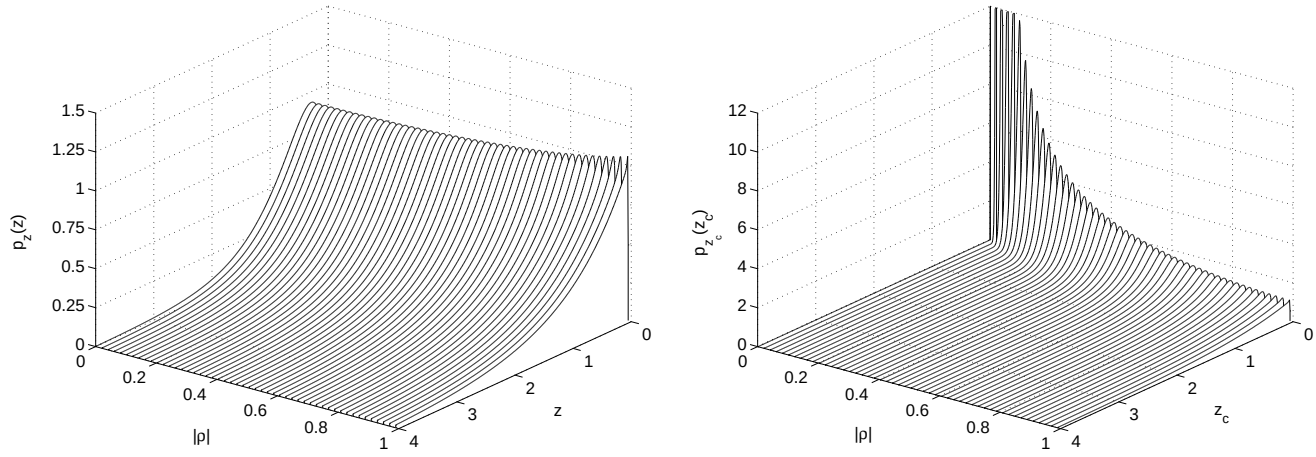

(a) (b)

Figure 5.2: Evolution, as a function of $|\rho|$, of the distributions: (a) $p_z(z)$ and (b) $p_{z_c}(z_c)$. In the second case, plots have been truncated for visualization convenience.

Fig. 5.2 depicts, for normalized power (i.e., $\psi = 1$), the distributions $p_z(z)$ and $p_{z_c}(z_c)$ for the whole coherence range, displaying which is the final effect of the parameter N_c, transforming $p_z(z)$ to $p_{z_c}(z_c)$. Noticeable differences can be observed at medium and low coherences. With the introduction of the random process z_c, the first additive term of Hermitian product real and imaginary parts are transformed to

$$\Re\{ze^{j\phi}\}_1 = z_c\cos(\phi_x) \tag{5.31}$$
$$\Im\{ze^{j\phi}\}_1 = z_c\sin(\phi_x). \tag{5.32}$$

Useful information is contained in the mean value of the terms $z_c\cos(\phi_x)$ and $z_c\sin(\phi_x)$. The expression of these can be easily derived from the mean value of the Hermitian product amplitude. The value corresponding to the real part term, Eq. (5.31), is derived as follows

$$\begin{aligned} E\left\{\Re\{ze^{j\phi}\}_1\right\} &= E\{z_c\}\cos(\phi_x) = N_c E\{z\}\cos(\phi_x) \\ &= \psi N_c\frac{\pi}{4}\,{}_2F_1\left(-\frac{1}{2},-\frac{1}{2};1;|\rho|^2\right)\cos(\phi_x) \\ &= \psi N_c\overline{z}_n\cos(\phi_x). \end{aligned} \tag{5.33}$$

The term $\overline{z}_n$ denotes the expected value of the Hermitian product normalized amplitude, whose value can be obtained from Eq. (5.11) setting $\psi = 1$. The second moment of $\Re\{ze^{j\phi}\}_1$ is obtained in the same way

$$\begin{aligned} E\left\{\Re\{ze^{j\phi}\}_1^2\right\} &= E\{z_c^2\}\cos^2(\phi_x) = N_c^2 E\{z^2\}\cos^2(\phi_x) \\ &= \psi^2 N_c^2(1+|\rho|^2)\cos^2(\phi_x). \end{aligned} \tag{5.34}$$

Consequently, the variance of the first additive term of the Hermitian product real part has the following expression

$$\begin{aligned} \mathrm{var}\left\{\Re\{ze^{j\phi}\}_1\right\} &= E\left\{\Re\{ze^{j\phi}\}_1^2\right\} - \left(E\left\{\Re\{ze^{j\phi}\}_1\right\}\right)^2 \\ &= \psi^2 N_c^2\left(1+|\rho|^2-\left(\frac{\pi}{4}\right)^2\,{}_2F_1^2\left(-\frac{1}{2},-\frac{1}{2};1;|\rho|^2\right)\right)\cos^2(\phi_x). \end{aligned} \tag{5.35}$$

Fig. 5.3a depicts $E\left\{\Re\{ze^{j\phi}\}_1\right\}$ for normalized power (i.e., $\psi = 1$) and $\cos(\phi_x) = 1$. Considering equations Eq. (5.33) for $E\left\{\Re\{ze^{j\phi}\}_1\right\}$, and Eq. (5.23) for $E\{z_R\}$, some similarities can be noticed. In this case,

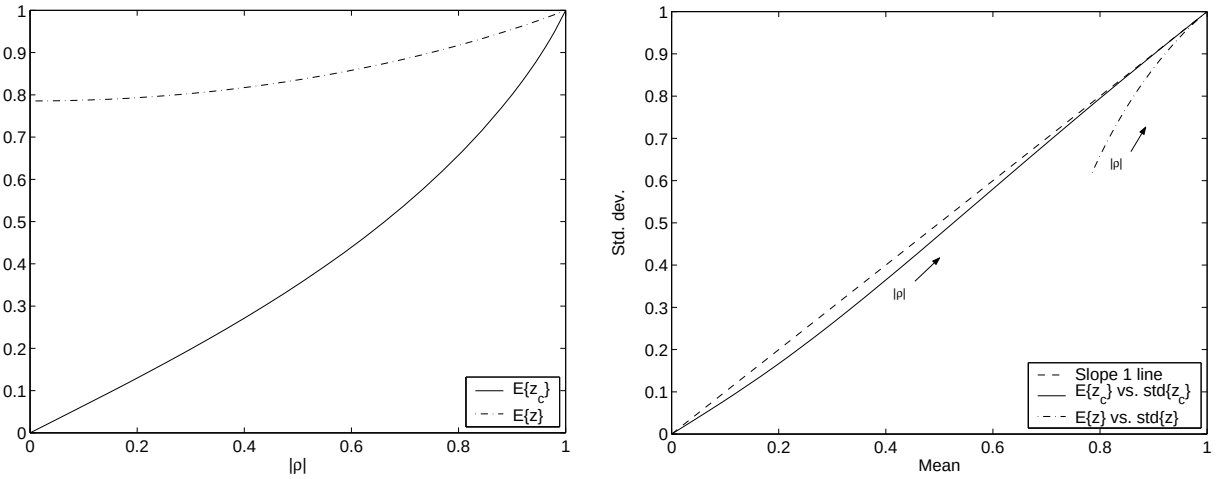

(a) (b)

Figure 5.3: (a) $E\left\{\Re\{ze^{j\phi}\}_1\right\}$ as a function of coherence $|\rho|$. (b) Standard deviation as a function of the mean for the Hermitian product amplitude and the term $\Re\{ze^{j\phi}\}_1$. In both cases $\psi = 1$ and $\cos(\phi_x) = 1$. The direction of increasing $|\rho|$ is indicated.

the terms $N_c\overline{z}_n$ and $|\rho|$ have the same role. This similarity is due to the fact that the parameter N_c and the coherence $|\rho|$ present close values, forcing for instance $E\left\{\Re\{ze^{j\phi}\}_1\right\}$ to be zero for $|\rho| = 0$.

Given an arbitrary random process, its mean value is usually referred as the information term, whereas the random variation around it is understood as noise. Consequently, the noise nature can be investigated by considering the relation between the mean value and the standard deviation, as the later takes into account the noise effects. This analysis is performed by means of Fig. 5.3b. In this case, the dashed line represents the relation corresponding to a random process whose standard deviation equals his mean value. In this situation, the process can be understood as a mean value multiplied by a random process with mean and standard deviation values equal to one. The solid line represents $\text{std}\left\{\Re\{ze^{j\phi}\}_1\right\}$ as a function of $E\left\{\Re\{ze^{j\phi}\}_1\right\}$, where std$\{\cdot\}$ stands for standard deviation. As Fig. 5.3b demonstrates, this relation is very close to the equality relation. For completeness, the relation between std$\{z\}$ and $E\{z\}$ for the Hermitian product amplitude, represented by the dash-dotted line, has also been included.

Given the graphics depicted in Fig. 5.3b, one can observe which is the final effect of the parameter N_c. In the case of the amplitude relation for the complex Hermitian product (i.e., dash-dotted line), a clear connection can not be established between the mean and the standard deviation values. But, if the parameter N_c is considered (i.e., solid line), the relation between the mean and the standard deviation turns to an almost equality relation. Let be the random process $\Re\{ze^{j\phi}\}_1$, if the standard deviation value is approximated by the corresponding mean value, that is

$$\text{std}\left\{\Re\{ze^{j\phi}\}_1\right\} \simeq \text{abs}\left(E\left\{\Re\{ze^{j\phi}\}_1\right\}\right) \tag{5.36}$$

where abs$(\cdot)$ denotes the absolute value then, the process $\Re\{ze^{j\phi}\}_1$ can be regarded as a deterministic term, equal to the average value $\psi N_c\overline{z}_n\cos(\phi_x)$, multiplied by a random term, denoted by n_m

$$\Re\{ze^{j\phi}\}_1 = z_c\cos(\phi_x) = \psi N_c\overline{z}_n n_m\cos(\phi_x). \tag{5.37}$$

Therefore, the random term n_m can be considered as a multiplicative noise term, such that $E\{n_m\} = 1$ and $\text{var}\{n_m\} = \sigma^2_{n_m} = 1$. The equivalent expression for the imaginary part is obtained as

$$\Im\{ze^{j\phi}\}_1 = z_c\sin(\phi_x) = \psi N_c\overline{z}_n n_m\sin(\phi_x). \tag{5.38}$$

In Fig. 5.4, one can observe the absolute error Δ std$\{\Re\{ze^{j\phi}\}_1\}$ which is introduced considering the standard deviation to be equal to the mean value instead of his actual value. Since the random behavior

of the first Hermitian product additive term is induced by the amplitude z, it only affects the final amplitude information, whereas it does not introduce noise in the phase difference ϕ_x. This effect can be seen easily under a complex formulation of the first additive term

$$\{ze^{j\phi}\}_1 = \psi N_c \overline{z}_n n_m e^{j\phi_x}. \tag{5.39}$$

Finally, as it can be deduced from this expression, the power term ψ only introduces an scaling factor without altering the multiplicative nature of n_m. Similarly, the true phase difference phasor introduces a rotation effect which does also not affect this multiplicative nature.

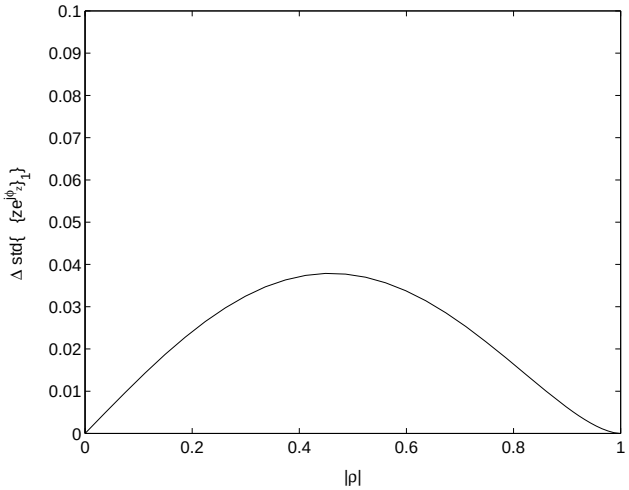

Figure 5.4: Absolute error introduced by the approximation of the standard deviation of the first additive term of the Hermitian product real part, $\Delta \operatorname{std}\left\{\Re\{ze^{j\phi}\}_1\right\} = E\left\{\Re\{ze^{j\phi}\}_1\right\} - \operatorname{std}\left\{\Re\{ze^{j\phi}\}_1\right\}$. The parameters ψ and $\cos(\phi_x)$ are assumed to be equal to 1.

5.4.2 Analysis of $zv_1' \exp(j\phi_x)$

The second additive term of Eq. (5.17) makes reference to the components

$$\Re\{ze^{j\phi}\}_2 = zv_1' \cos(\phi_x) \tag{5.40}$$
$$\Im\{ze^{j\phi}\}_2 = zv_1' \sin(\phi_x). \tag{5.41}$$

As it has been performed in the previous section, only the analysis corresponding to the real part case, Eq. (5.40), is presented in depth since the one corresponding to the imaginary part is obtained by interchanging the $\cos(\phi_x)$ and $\sin(\phi_x)$ terms. Unlike the first additive term analyzed in the preceding section, this term depends on two random components: the Hermitian product amplitude z and the phase term v_1' which has been defined in Section 4.2 at Chapter 4. This double dependence can be analyzed by introducing a new random process

$$z_1 = zv_1' = z(\cos(\phi) - N_c). \tag{5.42}$$

In this case, the term ϕ does not contain useful phase information as it has been included in other terms, see Eqs. (5.40) and (5.41). Consequently, the distribution corresponding to the process z_1 can be obtained by considering the distribution $p_{z,\phi}(z,\phi)$, Eq. (5.9), evaluated at $\phi_x = 0$ rad. The distribution $p_{z_1}(z_1)$ is obtained as follows

$$p_{z_1}(z_1) = \int_{-\pi}^{\pi} p_{z_1,\phi}(z_1,\phi)\,\mathrm{d}\phi = \int_{-\pi}^{\pi} p_{z,\phi}(z,\phi)|_{z=\frac{z_1}{\cos(\phi)-N_c}}\,\mathrm{d}\phi \qquad z_1 \in (-\infty,\infty). \tag{5.43}$$

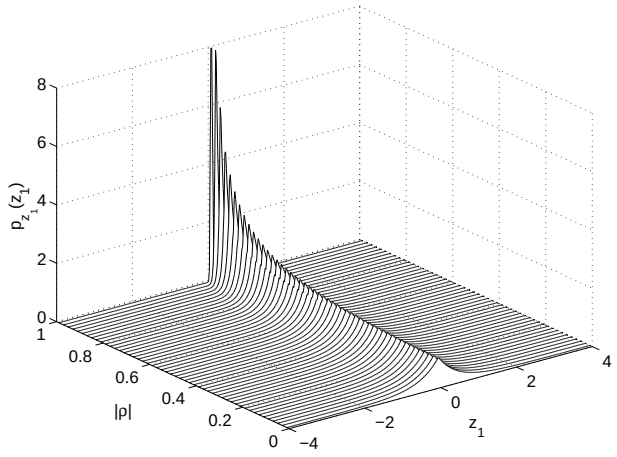

Figure 5.5: Distribution $p_{z_1}(z_1)$ for the whole coherence range.

The expression corresponding to $p_{z_1,\phi}(z_1,\phi)$ can be derived easily by introducing the change of variable presented by Eq. (5.42) into the distribution given by Eq. (5.9)

$$p_{z_1,\phi}(z_1,\phi) = \frac{2z_1\,\mathrm{sgn}(\cos(\phi)-N_c)}{\pi\psi^2(1-|\rho|^2)(\cos(\phi)-N_c)^2}\exp\left(\frac{2|\rho|z_1\cos(\phi)}{\psi(1-|\rho|^2)(\cos(\phi)-N_c)}\right) K_0\left(\frac{2z_1}{\psi(1-|\rho|^2)(\cos(\phi)-N_c)}\right). \tag{5.44}$$

where $\mathrm{sgn}(\cdot)$ denotes the sign function. Due to the complexity of Eq. (5.44), a closed expression for $p_{z_1}(z_1)$ can not be derived. Nevertheless, numerical methods can be employed to obtain it. Fig. 5.5 depicts the pdf $p_{z_1}(z_1)$ for the whole coherence range considering normalized power (i.e., $\psi=1$). Despite a closed expression for $p_{z_1}(z_1)$ can not be obtained for the complete coherence range, it is possible to derive it for the limit coherence values. The expression corresponding to $|\rho|=0$ is obtained by taking into account that z_1 simplifies to $z\cos(\phi)$, since for this coherence $N_c=0$. This case corresponds to the pdf of the Hermitian product real part for $|\rho|=0$, see Eq. (5.19). Consequently, the expressions of $p_{z_1}(z_1)$ for the coherence extreme values are

$$\lim_{|\rho|\to 0} p_{z_1}(z_1) = \frac{1}{\psi}\left(\exp\left(-\frac{2z_1}{\psi}\right)H(z_1)+\exp\left(\frac{2z_1}{\psi}\right)H(-z_1)\right) \qquad z_1\in(-\infty,\infty) \tag{5.45}$$

$$\lim_{|\rho|\to 1} p_{z_1}(z_1) = \delta(0) \qquad z_1\in(-\infty,\infty). \tag{5.46}$$

A first comparison of the previous two equation with the equivalent ones corresponding the first additive term of the Hermitian product real part, Eqs. (5.29) and (5.30), shows that both additive terms present an opposite behavior, since whereas the first additive term cancels out for low coherences, the second additive term cancels out for high ones.

The second additive terms, corresponding to the real and imaginary parts of the Hermitian product, can be expressed as follows

$$\Re\{ze^{j\phi}\}_2 = z_1\cos(\phi_x) \tag{5.47}$$

$$\Im\{ze^{j\phi}\}_2 = z_1\sin(\phi_x). \tag{5.48}$$

The mean and variance values of the previous two terms can be obtained either through numeric procedures employing Eq. (5.43), or by considering Eq. (5.42), which allows to derive theoretical expressions as a function of the different signal parameters. The mean value corresponding to the real part case, Eq.

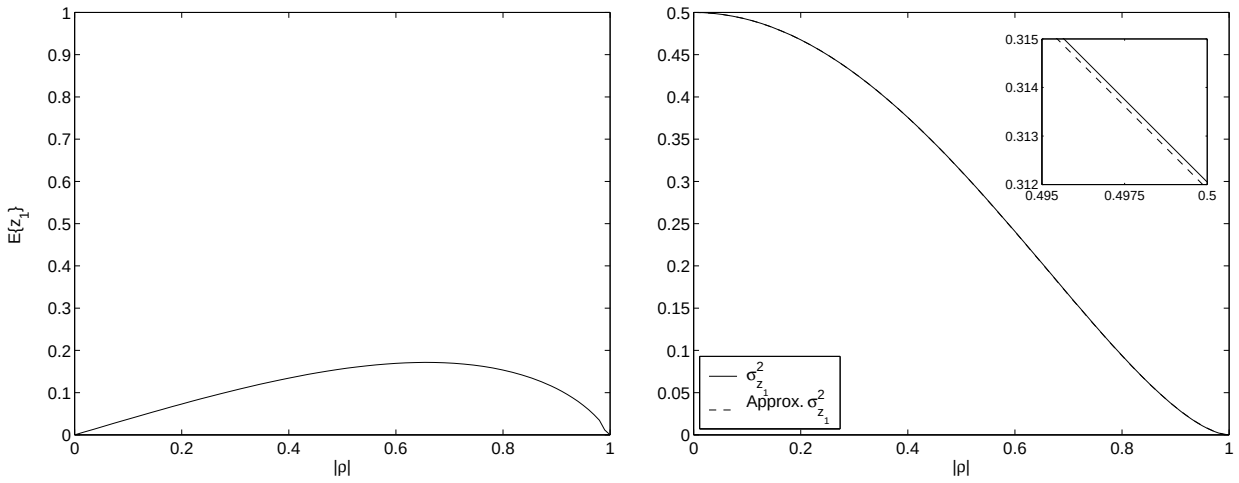

(a) (b)

Figure 5.6: (a) $E\left\{\Re\{ze^{j\phi}\}_2\right\}$ a as function of coherence $|\rho|$. (b) Actual and approximated values of $\text{var}\left\{\Re\{ze^{j\phi}\}_2\right\}$ for the whole coherence range. A detail around $|\rho| = 0.5$ is also presented. In both cases one assumes $\psi = 1$ and $\cos(\phi_x) = 1$.

(5.47), has the expression

$$\begin{aligned} E\left\{\Re\{ze^{j\phi}\}_2\right\} &= (E\{z\cos(\phi)\} - N_c E\{z\})\cos(\phi_x) \\ &= \psi\left(|\rho| - N_c\overline{z}_n\right)\cos(\phi_x) \\ &= \psi\left(|\rho| - N_c\frac{\pi}{4}\,{}_2F_1\left(-\frac{1}{2},-\frac{1}{2};1;|\rho|^2\right)\right)\cos(\phi_x). \end{aligned} \tag{5.49}$$

Fig. 5.6a presents a graphic of $E\left\{\Re\{ze^{j\phi}\}_2\right\}$ for the normalized power case (i.e., $\psi = 1$), and considering $\cos(\phi_x) = 1$. From this figure, one observes that the mean value of this term is always lower than 0.2. The addition of the mean values of the first and second additive terms, Eqs. (5.33) and (5.49), corresponds to the mean value of the Hermitian product real part, Eq. (5.23). Consequently, it can be affirmed that the useful information to retrieve is distributed between the first and the second additive terms of the Hermitian product real and imaginary parts, being the first additive term the one which contains a larger part of it.

The second moment of $\Re\{ze^{j\phi}\}_2$ is obtained as follows

$$\begin{aligned} E\left\{\Re\{ze^{j\phi}\}_2^2\right\} &= E\{z_1^2\}\cos^2(\phi_x) = E\{z^2(\cos(\phi) - N_c)^2\}\cos^2(\phi_x) \\ &= \left(E\{(z\cos(\phi))^2\} + N_c^2 E\{z^2\} - 2N_c E\{z^2\cos(\phi)\}\right)\cos^2(\phi_x). \end{aligned} \tag{5.50}$$

The term $E\{(z\cos(\phi))^2\}$ corresponds to the second moment of the Hermitian product real part for $\phi_x = 0$ rad. Consequently, this value can be obtained straightforwardly from Eq. (5.24). Since N_c is a constant value, the second term, $N_c^2 E\{z^2\}$, corresponds to the second moment of the Hermitian product amplitude, whose value is given by Eq. (5.12). Finally, the expression of the term $E\{z^2\cos(\phi)\}$ is obtained by integrating the function $z^2\cos(\phi)$ with respect to the pdf $p_{z,\phi}(z,\phi)$. Appendix E concerns the calculation of this expression. Thus, $E\left\{\Re\{ze^{j\phi}\}_2^2\right\}$ follows

$$\begin{aligned} &E\left\{\Re\{ze^{j\phi}\}_2^2\right\} \\ &= \psi^2\left[\frac{1}{2}(1-|\rho|^2) + 2|\rho|^2 + N_c^2 + N_c^2|\rho|^2 - N_c|\rho|\frac{9\pi}{8}\,{}_2F_1\left(-\frac{1}{2},-\frac{1}{2};2;|\rho|^2\right)\right]\cos^2(\phi_x). \end{aligned} \tag{5.51}$$

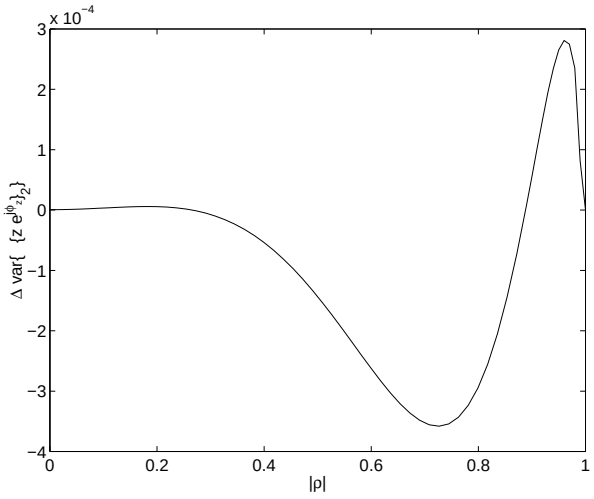

Figure 5.7: Absolute error of the approximated value of $\text{var}\left\{\Re\{ze^{j\phi}\}_2\right\}$ obtained as $\Delta\,\text{var}\left\{\Re\{ze^{j\phi}\}_2\right\} = \frac{1}{2}\psi(1-|\rho|^2)^{1.64}\cos^2(\phi_x) - \text{var}\left\{\Re\{ze^{j\phi}\}_2\right\}$. Also for this case the parameters ψ and $\cos(\phi_x)$ are assumed to be equal to 1.

From Eqs. (5.49) and (5.51), the variance of the term $\Re\{ze^{j\phi}\}_2$ is derived as follows

$$\begin{aligned}
&\text{var}\left\{\Re\{ze^{j\phi}\}_2\right\} = E\left\{\Re\{ze^{j\phi}\}_2^2\right\} - \left(E\left\{\Re\{ze^{j\phi}\}_2\right\}\right)^2 \\
= \;& \psi^2\left[\frac{1}{2}(1-|\rho|^2) + 2|\rho|^2 + N_c^2 + N_c^2|\rho|^2 - N_c|\rho|\frac{9\pi}{8}{}_2F_1\left(-\frac{1}{2},-\frac{1}{2};2;|\rho|^2\right)\right. \\
- \;& \left.\left(|\rho| - N_c\frac{\pi}{4}{}_2F_1\left(-\frac{1}{2},-\frac{1}{2};1;|\rho|^2\right)\right)^2\right]\cos^2(\phi_x). \qquad (5.52)
\end{aligned}$$

From the previous equation, it is not evident to extract a conclusion with respect to the dependence of $\text{var}\left\{\Re\{ze^{j\phi}\}_2\right\}$ on the coherence $|\rho|$. Fig. 5.6b depicts the variance of the second additive term for the whole coherence range, considering $\psi = 1$ and $\cos(\phi_x) = 1$.

The term zv_1' is a function of the phase difference term v_1'. If one makes a qualitative comparison between the variance of v_1', Eq. (4.14) and Fig. 4.2a, and the variance of zv_1', Eq. (5.52) and Fig. 5.6b, one can deduce that both quantities present approximately the same dependence with respect to the coherence $|\rho|$. Therefore, the family of functions given by Eq. (4.12) is also employed to approximate the value of $\text{var}\left\{\Re\{ze^{j\phi}\}_2\right\}$. In the same manner as it has been obtained within the previous chapter, one founds that the family of curves given by Eq. (4.12), on page 78, minimizes the mean square error between the actual an the approximated value for $\text{var}\left\{\Re\{ze^{j\phi}\}_2\right\}$ for the exponent $\alpha = 1.64$. Fig. 5.6b shows the approximated value superimposed to the actual values of $\text{var}\left\{\Re\{ze^{j\phi}\}_2\right\}$, where it can be observed the closeness between them. Fig. 5.7 presents the absolute error between the actual and the approximated variance values for the second additive term of the Hermitian product real part, showing the approximation accuracy. Finally, the approximated expression for $\text{var}\left\{\Re\{ze^{j\phi}\}_2\right\}$ follows

$$\text{var}\left\{\Re\{ze^{j\phi}\}_2\right\} \simeq \frac{1}{2}\psi^2(1-|\rho|^2)^{1.64}\cos^2(\phi_x). \qquad (5.53)$$

As it has been presented, the term $\Re\{ze^{j\phi}\}_2$ can be regarded as a deterministic term corresponding to the mean value, Eq. (5.49), plus a zero-mean random term, termed n_{a1} in the following, whose variance value depends on Eq. (5.53). Consequently, the term $\Re\{ze^{j\phi}\}_2$ can be written as follows

$$\Re\{ze^{j\phi}\}_2 = \psi\left[(|\rho| - N_c\overline{z}_n) + n_{a1}\right]\cos(\phi_x). \qquad (5.54)$$

In the same way, the imaginary part of the Hermitian product second additive term, Eq. (5.41) can be also written as

$$\Im\{ze^{j\phi}\}_2 = \psi\left[(|\rho| - N_c\overline{z}_n) + n_{a1}\right]\sin(\phi_x). \qquad (5.55)$$

In the light of the previous results, the term n_{a1} corresponds to an additive noise term such that $E\{n_{a1}\} = 0$ and whose variance corresponds, considering the approximation introduced in Eq. (5.53), to

$$\text{var}\{n_{a1}\} = \sigma^2_{n_{a1}} = \frac{\text{var}\left\{\Re\{ze^{j\phi}\}_2\right\}}{\psi^2\cos^2(\phi_x)} = \frac{1}{2}(1-|\rho|^2)^{1.64}. \tag{5.56}$$

Since the random process n_{a1} is the same for the real and imaginary parts of the Hermitian product second additive term, this term can be written under a complex formulation as

$$\{ze^{j\phi}\}_2 = \psi\left[(|\rho| - N_c\overline{z}_n) + n_{a1}\right]e^{j\phi_x}. \tag{5.57}$$

Unlike the term analyzed within the preceding section, in this case an additive noise term n_{a1} has been identified, in contrast with the multiplicative noise term n_m identified in the previous case.

5.4.3 Analysis of $jzv_2'\exp(j\phi_x)$

This section analyzes the third term of the Hermitian product real and imaginary parts, Eqs. (5.15) and (5.16), whose expressions are

$$\Re\{ze^{j\phi}\}_3 = -zv_2'\sin(\phi_x) \tag{5.58}$$
$$\Im\{ze^{j\phi}\}_3 = zv_2'\cos(\phi_x). \tag{5.59}$$

Just as one will see throughout the analysis of the previous two equations, the third additive term of the Hermitian product is qualitatively very similar to the second additive term analyzed in Section 5.4.2. In this case, the randomness of this term is determined by the Hermitian product amplitude z and the phase difference term v_2', which corresponds to the term $\sin(\phi)$, instead to $\cos(\phi)$ as it happens for the second additive term. Consequently, an additional random process can be introduced as follows

$$z_2 = zv_2' = z\sin(\phi). \tag{5.60}$$

As it can be observed, the random process z_2 corresponds to the imaginary part of the Hermitian product evaluated at the phase difference $\phi_x = 0$ rad. Consequently, its statistical behavior is fully determined by the pdf of the Hermitian product imaginary part. Considering Eq. (5.20) for the Hermitian product imaginary part evaluated at $\cos(\phi_x) = 1$, the distribution of z_2, referred as $p_{z_2}(z_2)$ has the expression

$$p_{z_2}(z_2) = \frac{1}{2\sqrt{1-|\rho|^2}}\left(\exp\left(-\frac{2z_2\sqrt{1-|\rho|^2}}{\psi(1-|\rho|^2)}\right)H(z_2) + \exp\left(\frac{2z_2\sqrt{1-|\rho|^2}}{\psi(1-|\rho|^2)}\right)H(-z_2)\right) \quad z_2 \in (-\infty,\infty) \tag{5.61}$$

where $H(x)$ represents the Heaviside step function. Fig. 5.8 represents the pdf $p_{z_2}(z_2)$ for the complete coherence range. Comparing Fig. 5.8 with the corresponding one to the random process z_1, Fig. 5.5, one can observe that both pdfs present a very similar behavior for any coherence value. Indeed, the expressions of $p_{z_2}(z_2)$ for the extreme coherence values

$$\lim_{|\rho|\to 0} p_{z_2}(z_2) = \frac{1}{\psi}\left(\exp\left(-\frac{2z_2}{\psi}\right)H(z_2) + \exp\left(\frac{2z_2}{\psi}\right)H(-z_2)\right) \qquad z_2 \in (-\infty,\infty) \tag{5.62}$$
$$\lim_{|\rho|\to 1} p_{z_2}(z_2) = \delta(0) \qquad z_2 \in (-\infty,\infty) \tag{5.63}$$

are respectively the same as the pdfs for the random process z_1, Eqs. (5.45) and (5.46).

As it has been performed for the other terms of the Hermitian product real and imaginary parts, the third additive terms can be written as

$$\Re\{ze^{j\phi}\}_3 = -z_2\sin(\phi_x) \tag{5.64}$$
$$\Im\{ze^{j\phi}\}_3 = z_2\cos(\phi_x). \tag{5.65}$$

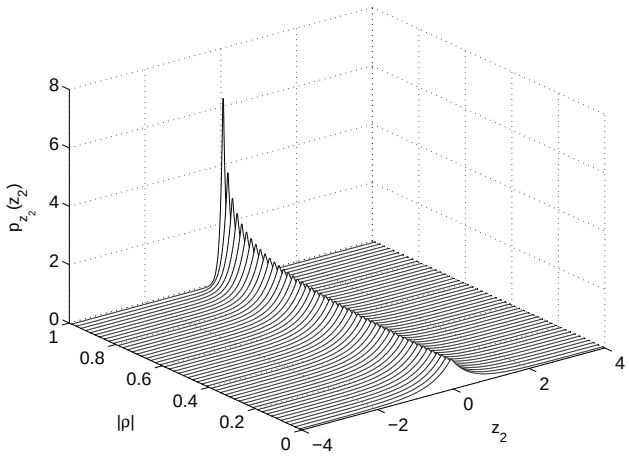

Figure 5.8: Pdf $p_{z_2}(z_2)$ as a function of coherence. The power parameter ψ, and the phase parameter $\cos(\phi_x)$ are assumed to be equal to 1.

Since the random behavior of these two terms is completely determined by the random process z_2, which has been shown very similar to the random term z_1, Eqs. (5.64) and (5.65) will present a very similar behavior to the second additive terms of the Hermitian product real and imaginary parts. The most important difference between the second and the third additive term is found under a complex formulation, since the third additive term presents a $\pi/2$ rad rotation with respect to the second additive term. This relative rotation between the second and the third additive terms will be employed later to simplify the final speckle noise model for the complex Hermitian product of SAR images.

The moments of the terms given by Eqs. (5.64) and (5.65) are analyzed in the following. As it has been done throughout the preceding section, only the expression for the real part case is given, as the imaginary part moments can be derived by simply interchanging the $\cos(\phi_x)$ and $\sin(\phi_x)$ terms. At the beginning of the current section, it has been shown that the random term z_2 corresponds to the imaginary part of the Hermitian product evaluated at $\phi_x = 0$ rad. Consequently, the mean value of $\Re\{ze^{j\phi}\}_3$ can be derived from Eq. (5.23), interchanging $\cos(\phi_x)$ by $\sin(\phi_x)$, and evaluating it at $\phi_x = 0$ rad. Therefore

$$E\{\Re\{ze^{j\phi}\}_3\} = -E\{z_2\}\sin(\phi_x) = 0. \tag{5.66}$$

It has to be mentioned that the term $\sin(\phi_x)$ can take, in this case, any value since the evaluation at $\phi_x = 0$ rad is only employed to derive the pdf of the term z_2. Therefore, $E\{\Re\{ze^{j\phi}\}_3\}$ is zero due to $E\{z_2\} = 0$; it can be observed that the pdf $p_{z_2}(z_2)$ is symmetric about zero, explaining hence Eq. (5.66). Comparing Eq. (5.66) with Eq. (5.49), one observes a clear difference between them as the later presents values different from zero, despite it is always lower than 0.2. The main consequence of this difference is that the third additive term does not contain useful information at all. Hence, it can be regarded as a pure additive noise term. By the same procedure employed to obtain $E\{\Re\{ze^{j\phi}\}_3\}$, the second moment is derived as follows

$$E\{\Re\{ze^{j\phi}\}_3^2\} = E\{z_2^2\}\sin^2(\phi_x) = \frac{1}{2}\psi^2(1-|\rho|^2)\sin^2(\phi_x). \tag{5.67}$$

The variance, is straightforwardly obtained as

$$\mathrm{var}\{\Re\{ze^{j\phi}\}_3\} = \frac{1}{2}\psi^2(1-|\rho|^2)\sin^2(\phi_x). \tag{5.68}$$

Regardless of the power and phase dependence, the term $\mathrm{var}\{\Re\{ze^{j\phi}\}_3\}$ belongs to the family of functions which have been employed successfully to approximate the variance of different random processes, Eq. (4.12). In this case, the exponent α equals 1.

Taking into consideration Eqs. (5.66) and (5.68), the term $\Re\{ze^{j\phi}\}_3$ can be considered, hence, as a zero-mean, additive random term for the Hermitian product real part. In the same way as it has been

performed in Section 5.4.2, a new random process n_{a2} is defined. Consequently, the third additive term of the Hermitian product real part can be written as

$$\Re\{ze^{j\phi}\}_3 = -\psi n_{a2}\sin(\phi_x) \tag{5.69}$$

whereas the imaginary part follows

$$\Im\{ze^{j\phi}\}_3 = \psi n_{a2}\cos(\phi_x). \tag{5.70}$$

The additive noise term n_{a2} has a mean equal to $E\{n_{a2}\} = 0$ and his variance has the expression

$$\text{var}\{n_{a2}\} = \sigma^2_{n_{a2}} = \frac{\text{var}\left\{\Re\{ze^{j\phi}\}_3\right\}}{\psi^2\sin^2(\phi_x)} = \frac{1}{2}(1-|\rho|^2). \tag{5.71}$$

Considering Eqs. (5.69) and (5.70) under a complex formulation, the third additive term of the Hermitian product of correlated SAR images has the following expression

$$\{ze^{j\phi}\}_3 = j\psi n_{a2}e^{j\phi_x}. \tag{5.72}$$

5.4.4 Joint Moments

Throughout the previous sections, it has been demonstrated that the real and imaginary parts of the Hermitian product of two correlated SAR images can be split up into three different additive terms. As presented, it is possible to identify different noise sources in each of these terms. This section concerns a study of the covariance properties between these three additive terms. Since the single difference between the real and the imaginary parts of the Hermitian product is on the effect of the true phase difference term $\cos(\phi_x)$ and $\sin(\phi_x)$, a detailed study will be performed only over the real part. The results concerning the imaginary part are derived by an interchange of the $\cos(\phi_x)$ and $\sin(\phi_x)$ terms.

First, the correlation properties between the first and the second additive terms of the Hermitian product real part will be analyzed. This correlation is studied by considering the covariance term defined as

$$\mathcal{C}_{12} = E\left\{(\Re\{ze^{j\phi}\}_1 - E\{\Re\{ze^{j\phi}\}_1\})(\Re\{ze^{j\phi}\}_2 - E\{\Re\{ze^{j\phi}\}_2\})\right\}. \tag{5.73}$$

Considering the random processes z_c and z_1, introduced by Eqs. (5.27) and (5.42), the covariance $\mathcal{C}_{12}$ takes the form

$$\begin{aligned}\mathcal{C}_{12} &= E\left\{(z_c\cos(\phi_x) - E\{z_c\cos(\phi_x)\})(z_1\cos(\phi_x) - E\{z_1\cos(\phi_x)\})\right\}\\ &= E\left\{(z_c - E\{z_c\})(z_1 - E\{z_1\})\right\}\cos^2(\phi_x)\\ &= (E\{z_cz_1\} - E\{z_c\}E\{z_1\})\cos^2(\phi_x)\end{aligned} \tag{5.74}$$

where it has been assumed that useful signal as well as random properties are homogeneous. The expression of the mean values $E\{z_c\}$ and $E\{z_1\}$ can be derived easily from the expressions given by Eqs. (5.33) and (5.49), respectively. The value of the joint first moment, $E\{z_cz_1\}$, is derived by considering the expression of the random processes z_c and z_1, Eqs. (5.27) and (5.42) respectively. Hence,

$$E\{z_cz_1\} = E\{zN_cz(\cos(\phi) - N_c)\} = N_c\left(E\{z^2\cos(\phi)\} - N_cE\{z^2\}\right). \tag{5.75}$$

The value of the term $E\{z^2\cos(\phi)\}$ is found on Appendix E, whereas the expectation value $E\{z^2\}$ corresponds to the second moment of the Hermitian product amplitude, see Eq. (5.12). Finally, introducing Eq. (5.75) into (5.74), and substituting the corresponding expressions, the covariance term $\mathcal{C}_{12}$ takes the form

$$\begin{aligned}\mathcal{C}_{12} &= \psi^2N_c\left[|\rho|\frac{9\pi}{16}\,{}_2F_1\left(-\frac{1}{2},-\frac{1}{2};2;|\rho|^2\right) - N_c(1+|\rho|^2)\right.\\ &- \left.\frac{\pi}{4}\,{}_2F_1\left(-\frac{1}{2},-\frac{1}{2};1;|\rho|^2\right)\left(|\rho| - N_c\frac{\pi}{4}\,{}_2F_1\left(-\frac{1}{2},-\frac{1}{2};1;|\rho|^2\right)\right)\right]\cos^2(\phi_x).\end{aligned} \tag{5.76}$$

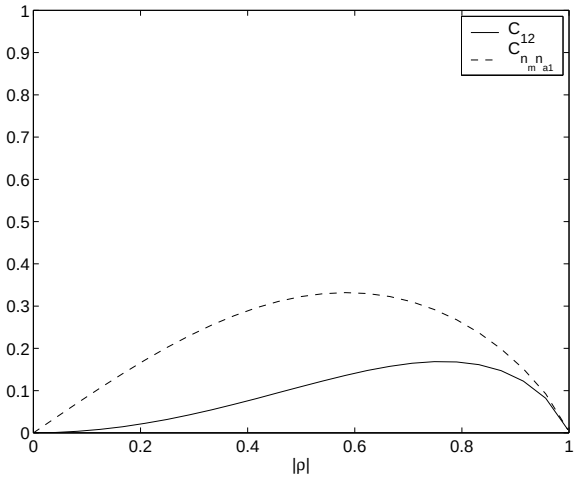

Figure 5.9: Covariances considering correlation properties between the first and the second additive terms of the Hermitian product. In this case: $\psi = 1$ and $\cos(\phi_x) = 1$.

As it comes out from the previous expression, it is difficult to discern the dependence of $\mathcal{C}_{12}$ on the coherence value $|\rho|$. As it has been observed in other terms throughout this chapter, the power parameter ψ, as well as the phase term $\cos(\phi_x)$ act as multiplicative terms. Fig. 5.9 presents the graphic of the covariance term $\mathcal{C}_{12}$ for the normalized power case (i.e., $\psi = 1$) as well as $\phi_x = 0$ rad. As it can be observed, the term $\mathcal{C}_{12}$ presents values which are lower than 0.2, presenting its maximum for a coherence value around 0.8.

From the covariance term $\mathcal{C}_{12}$ one can extract the covariance of the terms n_m and n_{a1}, referred as $\mathcal{C}_{n_m n_{a1}}$ in the following. These random processes have been defined as noise terms for the first and the second additive terms of the Hermitian product. Considering the expressions given by Eqs. (5.37) and (5.54), the expression corresponding to $\mathcal{C}_{n_m n_{a1}}$ is found to follow

$$\mathcal{C}_{n_m n_{a1}} = E\{(n_m - 1)n_{a1}\} = \frac{\mathcal{C}_{12}}{\psi^2 N_c \overline{z}_n \cos^2(\phi_x)}. \tag{5.77}$$

A plot of the covariance $\mathcal{C}_{n_m n_{a1}}$ as a function of the SAR images coherence can be observed in Fig. 5.9.

The second correlation term refers to the covariance which exists between the first an the third additive terms corresponding to the real part of the Hermitian product of correlated SAR images

$$\mathcal{C}_{13} = E\left\{(\Re\{ze^{j\phi}\}_1 - E\{\Re\{ze^{j\phi}\}_1\})(\Re\{ze^{j\phi}\}_3 - E\{\Re\{ze^{j\phi}\}_3\})\right\}. \tag{5.78}$$

Considering in this case the random process z_2 introduced in Eq. (5.60), the covariance term $\mathcal{C}_{13}$ is

$$\begin{aligned}
\mathcal{C}_{13} &= E\left\{(z_c\cos(\phi_x) - E\{z_c\cos(\phi_x)\})(-z_2\sin(\phi_x) - E\{-z_2\sin(\phi_x)\})\right\} \\
&= E\left\{(z_c - E\{z_c\})(-z_2 - E\{-z_2\})\right\}\cos(\phi_x)\sin(\phi_x) \\
&= (E\{z_c\}E\{z_2\} - E\{z_c z_2\})\cos(\phi_x)\sin(\phi_x).
\end{aligned} \tag{5.79}$$

As it is given by Eq. (5.66), $E\{z_2\} = 0$. In addition, as it is demonstrated at Appendix E, the joint expectation $E\{z_c z_2\} = 0$. Consequently, $\mathcal{C}_{13} = 0$ independently of the correlation between the pair of SAR images. As a result, the covariance between the noise terms n_m and n_{a2}, denoted by $\mathcal{C}_{n_m n_{a2}}$, is also zero.

The last correlation term to analyze refers to the covariance between the second and the third additive terms of the Hermitian product real part

$$\mathcal{C}_{23} = E\left\{(\Re\{ze^{j\phi}\}_2 - E\{\Re\{ze^{j\phi}\}_2\})(\Re\{ze^{j\phi}\}_3 - E\{\Re\{ze^{j\phi}\}_3\})\right\}. \tag{5.80}$$

The expression of $\mathcal{C}_{23}$ can be found considering the processes z_1 and z_2 as follows

$$\begin{aligned}\mathcal{C}_{23} &= E\left\{(z_1\cos(\phi_x) - E\{z_1\cos(\phi_x)\})(-z_2\sin(\phi_x) - E\{-z_2\sin(\phi_x)\})\right\} \\ &= E\left\{(z_1 - E\{z_2\})(-z_2 - E\{-z_2\}))\right\}\cos(\phi_x)\sin(\phi_x) \\ &= (E\{z_1\}E\{z_2\} - E\{z_1 z_2\})\cos(\phi_x)\sin(\phi_x). \end{aligned} \tag{5.81}$$

In Appendix E, it is demonstrated that the joint expectation $E\{z_1 z_2\} = 0$. Consequently, since $E\{z_2\} = 0$, the covariance term $\mathcal{C}_{23}$ is zero for any coherence value. As a result of this, the covariance between the two additive terms n_{a1} and n_{a2}, termed $\mathcal{C}_{n_{a1}n_{a2}}$, is zero.

The expressions for the covariance terms established between the different additive noise components for the Hermitian product real part $\mathcal{C}_{12}$, $\mathcal{C}_{13}$ and $\mathcal{C}_{23}$ are equally valid for the imaginary part by interchanging the $\cos(\phi_x)$ and $\sin(\phi_x)$ terms.

5.4.5 Hermitian Product Speckle Noise Model

At the beginning of this section, it was demonstrated that the real and imaginary parts of the Hermitian product of a pair of SAR images can be split into three additive terms as given by Eqs. (5.15) and (5.16). The following four sections were devoted to present an in-depth study of each one of these three additive terms, as well as their joint properties. The most important result of this analysis has been the possibility to identify different noise sources and to determine how them alter or damage the useful information content. Consequently, this section is devoted to study the Hermitian product as a combination of these three additive terms, giving, as a final result, the speckle noise model for the complex Hermitian product of a pair of SAR images.

For each one of three additive terms in which the real part of the Hermitian product has been divided, a model has been defined as given by Eqs. (5.37), (5.54) and (5.69). Thus, the real part of the Hermitian product can be written as

$$\begin{aligned}\Re\{ze^{j\phi}\} &= \Re\{ze^{j\phi}\}_1 + \Re\{ze^{j\phi}\}_2 + \Re\{ze^{j\phi}\}_3 \\ &= \psi N_c\overline{z}_n n_m\cos(\phi_x) + \psi\left[(|\rho| - N_c\overline{z}_n) + n_{a1}\right]\cos(\phi_x) - \psi n_{a2}\sin(\phi_x). \end{aligned} \tag{5.82}$$

Exactly in the same way, considering now the additive terms for the Hermitian product imaginary part, Eqs. (5.38), (5.55) and (5.70), it can be written as

$$\begin{aligned}\Im\{ze^{j\phi}\} &= \Im\{ze^{j\phi}\}_1 + \Im\{ze^{j\phi}\}_2 + \Im\{ze^{j\phi}\}_3 \\ &= \psi N_c\overline{z}_n n_m\sin(\phi_x) + \psi\left[(|\rho| - N_c\overline{z}_n) + n_{a1}\right]\sin(\phi_x) + \psi n_{a2}\cos(\phi_x). \end{aligned} \tag{5.83}$$

The real and imaginary parts of the Hermitian product of a pair of SAR images can be expressed in a more compact form by considering them in a complex formulation. Therefore, considering the additive terms in a complex form, Eqs. (5.39), (5.57) and (5.72), the Hermitian product of SAR images has the following expression

$$\begin{aligned}S_k S_l^* &= ze^{j\phi} = \{ze^{j\phi}\}_1 + \{ze^{j\phi}\}_2 + \{ze^{j\phi}\}_3 \\ &= \psi N_c\overline{z}_n n_m e^{j\phi_x} + \psi\left[(|\rho| - N_c\overline{z}_n) + n_{a1}\right]e^{j\phi_x} + j\psi n_{a2}e^{j\phi_x}. \end{aligned} \tag{5.84}$$

As it has been demonstrated, the noise term n_m refers to a multiplicative noise component, whereas the noise terms n_{a1} and n_{a2} refer to additive noise components. Table 5.1 summarizes the statistical properties of these noise terms.

The noise model given by Eq. (5.84) can be further simplified considering an idea already introduced in Section 4.2. On page 80, the processes v_c and v_s were defined as a function of the phase difference terms v_1' and v_2'. Since the additive noise terms n_{a1} and n_{a2} are generated by v_1' and v_2' respectively, and the Hermitian product amplitude z, they can be joined essentially in the same way as v_1' and v_2' are

		Mean, $E\{\cdot\}$	Variance, σ^2
Multiplicative noise term	n_m	1	1
Additive noise terms	n_{a1}	0	$\frac{1}{2}(1-\lvert\rho\rvert^2)^{1.64}$
	n_{a2}	0	$\frac{1}{2}(1-\lvert\rho\rvert^2)$

Table 5.1: Mean and variance values for the three noise sources identified in the Hermitian product of complex SAR images.

combined. Considering the real and imaginary parts of the Hermitian product, Eqs. (5.82) and (5.83), two additional random processes are defined as follows

$$\psi n_{ar} = \psi n_{a1}\cos(\phi_x) - \psi n_{a2}\sin\phi_x \tag{5.85}$$
$$\psi n_{ai} = \psi n_{a1}\sin(\phi_x) + \psi n_{a2}\cos\phi_x. \tag{5.86}$$

As given, the power term ψ introduces only an scaling factor. The mean values of these two new random processes are easily derived from the values presented in Table 5.1. Hence, considering that the signal, as well as the random terms are homogeneous

$$E\{n_{ar}\} = E\{n_{a1}\}\cos(\phi_x) - E\{n_{a2}\}\sin(\phi_x) = 0 \tag{5.87}$$
$$E\{n_{ai}\} = E\{n_{a1}\}\sin(\phi_x) + E\{n_{a2}\}\cos(\phi_x) = 0. \tag{5.88}$$

In order to derive the variance of the processes n_{ar} and n_{ai} two points have to be considered. First, in Section 5.4.4 it has been proved that the covariance term between n_{a1} and n_{a2}, $\mathcal{C}_{n_{a1}n_{a2}}$, is zero, see Eq. (5.81). Therefore the variance values, for an homogeneous signal, have the expressions

$$\text{var}\{n_{ar}\} = \text{var}\{n_{a1}\}\cos^2(\phi_x) + \text{var}\{n_{a2}\}\sin^2(\phi_x) \tag{5.89}$$
$$\text{var}\{n_{ai}\} = \text{var}\{n_{a1}\}\sin^2(\phi_x) + \text{var}\{n_{a2}\}\cos^2(\phi_x). \tag{5.90}$$

Second, as it can be observed in Table 5.1, the variances of n_{a1} and n_{a2} present very similar values. Fig. 5.10 gives a plot of both variance terms as a function of the coherence parameter. The phase terms $\cos(\phi_x)$ and $\sin(\phi_x)$ are complementary since $\cos^2(\phi_x)+\sin^2(\phi_x)=1$, and their values lie in the interval $[0,1]$. As a result, the next inequality becomes true

$$\sigma^2_{n_{a1}} \leq \left\{ \begin{array}{c} \sigma^2_{n_{ar}} \\ \sigma^2_{n_{ai}} \end{array} \right\} \leq \sigma^2_{n_{a2}}. \tag{5.91}$$

Considering the previous equation, one demonstrates that the variance of the new noise processes n_{ar} and n_{ai} is always between the corresponding values for the terms n_{a1} and n_{a2}. As given in Appendix C, if one wants to describe $\sigma^2_{n_{ar}}$ and $\sigma^2_{n_{ai}}$ by the same family of functions as $\sigma^2_{n_{a1}}$ and $\sigma^2_{n_{a2}}$, the exponent α should depend both on $|\rho|$ and ϕ_x. Due to the closeness between the values of $\sigma^2_{n_{a1}}$ and $\sigma^2_{n_{a2}}$, it was shown in the same Appendix that one can get rid of these dependencies by considering the average exponent at the expense of introducing an error on the variance values. In this case $\sigma^2_{n_{a1}}$ is described by a curve whose exponent α equals 1.64 and the exponent of the curve $\sigma^2_{n_{a2}}$ equals 1. Consequently, $\sigma^2_{n_{ar}}$ and $\sigma^2_{n_{ai}}$ can be described, according to Appendix C, by curves whose exponent equals 1.32

$$\sigma^2_{n_{ar}} = \sigma^2_{n_{ai}} = \frac{1}{2}(1-|\rho|^2)^{1.32}. \tag{5.92}$$

Fig. 5.10 depicts the graphic of the terms $\sigma^2_{n_{ar}}$ and $\sigma^2_{n_{ai}}$, where they can be compared with the curves corresponding to $\sigma^2_{n_{a1}}$ and $\sigma^2_{n_{a2}}$.

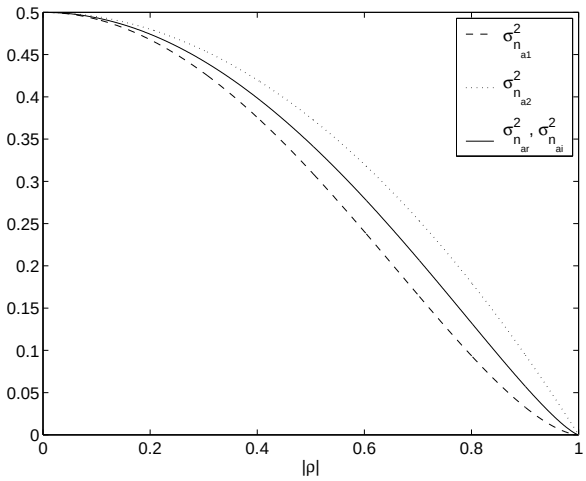

Figure 5.10: Graphics corresponding to the variances $\sigma^2_{n_{a1}}$, $\sigma^2_{n_{a2}}$, $\sigma^2_{n_{ar}}$ and $\sigma^2_{n_{ai}}$. These variances are described by curves of the type $\sigma^2 = (1/2)(1-|\rho|^2)^{\alpha}$, where α is 1.64, 1, 1.32 and 1.32 for each variance, respectively.

By introducing the definition of the noise processes $\sigma^2_{n_{ar}}$ and $\sigma^2_{n_{ai}}$ into the speckle noise model equations for the real and imaginary parts of the Hermitian product, Eqs. (5.82) and (5.83), the speckle noise model becomes

$$\Re\{ze^{j\phi}\} = \psi N_c \overline{z}_n n_m \cos(\phi_x) + \psi(|\rho| - N_c\overline{z}_n)\cos(\phi_x) + \psi n_{ar} \tag{5.93}$$

$$\Im\{ze^{j\phi}\} = \psi N_c \overline{z}_n n_m \sin(\phi_x) + \psi(|\rho| - N_c\overline{z}_n)\sin(\phi_x) + \psi n_{ai}. \tag{5.94}$$

These expressions can be joined under a complex formulation, yielding to the final speckle noise model for the complex Hermitian product of a pair of SAR images

$$S_k S_l^* = \psi N_c \overline{z}_n n_m e^{j\phi_x} + \psi(|\rho| - N_c\overline{z}_n)e^{j\phi_x} + \psi(n_{ar} + jn_{ai}). \tag{5.95}$$

A graphic view of the noise model given by Eq. (5.95) can be observed in Fig. 5.11.

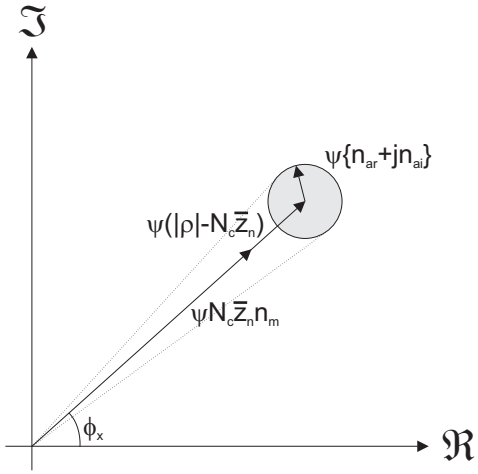

Figure 5.11: Graphical representation of the complex Hermitian product speckle noise model.

If Fig. 5.11 is compared with the figure corresponding to the Hermitian product phase difference phasor noise model, Fig. 4.6 on page 81, one can notice the similarity between both diagrams. Consequently, it can be concluded that the Hermitian speckle noise model is basically determined by the statistical behavior of the average phase difference.

5.4.6 Generalized Speckle Noise Model

Eq. (5.95) represents a speckle noise model for the Hermitian product of a pair of SAR images. As it can be seen, the terms n_m, n_{ar} and n_{ai} denote the noise sources which damage the useful signal content. Before to validate the speckle noise model proposed by Eq. (5.95), as well as to study its implications, it will be demonstrated that this model is in accordance with the speckle noise models existing until now. These noise models refer to the multiplicative speckle noise model for a SAR image intensity and to the additive noise model for the phase difference of two complex SAR images.

The speckle noise model for the Hermitian product considers a pair of complex SAR images S_k and S_l, whose correlation properties are determined by the complex correlation coefficient ρ. The SAR image intensity can be studied by considering the Hermitian product $S_k S_l^*$ where $k = l$. In this case, the complex correlation coefficient, obtained as given by Eq. (5.6), equals 1, that is, $|\rho| = 1$ and $\phi_x = 0$ rad. Consequently, the parameter N_c and the Hermitian product normalized amplitude $\overline{z}_n$ equal also 1, producing the term $|\rho| - N_c\overline{z}_n$ to be equal to zero. For $|\rho| = 1$, considering Eqs. (5.87), (5.88) and (5.92) one can deduce that the additive noise terms n_{ar} and n_{ai} cancel out as their mean, as well as their standard deviation values equal zero. Introducing $\rho = 1$, together with the associated consequences detailed in the previous lines, the complex Hermitian product speckle noise model reduces to

$$S_k S_k^* = |S_k|^2 = \psi n_m \tag{5.96}$$

where, in this case $\psi = E\{|S_k|^2\}$. Considering what has been presented in Section 2.1.6, it can be observed, that, the proposed speckle noise model for the Hermitian product of a pair of SAR images reduces to the well known multiplicative speckle noise model for the intensity of a SAR image when the product $S_k S_k^*$ is considered. Retaking the definition of the sample covariance matrix $[Z]$, Eq. (5.7), Eq. (5.95) is able, hence, to describe the nature of speckle noise for the diagonal, as well as for the off-diagonal elements of the sample covariance matrix.

Additionally, considering the statistical properties of the phase difference between two complex SAR images, it has been shown that speckle noise can be considered as an additive noise term, Eq. (4.1). As it has been shown in Section 5.3, the Hermitian product speckle noise model is derived precisely on the basis of the phase difference noise additivity. Consequently, Eq. (5.95) is also in accordance, by construction, with the speckle noise model for the phase difference of a pair of SAR images.

As a conclusion from which has been demonstrated in this section, the proposed speckle noise model for the complex Hermitian product of a pair of SAR images, Eq. (5.95), represents a generalization of the existing speckle noise models. Additionally, as mentioned in the introduction, the Hermitian product represents the building block to describe multidimensional SAR imagery under a covariance matrix formulation. Therefore, a general multidimensional speckle noise model can be defined on the basis of Eq. (5.95).

5.4.7 Multidimensional Speckle Noise Model

The aim of the present section is to obtain the expression for the multidimensional speckle noise model, under a covariance matrix formulation, on the basis of the Hermitian product speckle noise model given by Eq. (5.95). The main advantage of this approach lies in the fact that all the covariance matrix elements consist in the Hermitian product of two complex SAR images, allowing to obtain straightforwardly a multidimensional noise model expression for the sample covariance matrix $[Z]$.

Before to present the final expression for the multidimensional speckle noise model for PolSAR data, a first point has to be addressed. As the speckle noise model for the Hermitian product shows, Eq. (5.95), the speckle noise presents a multiplicative component given by n_m which damages the useful signal term $\psi N_c \overline{z}_n \exp(j\phi_x)$. The direct extension of this term to a matrix formulation is not possible since it cannot be expressed as the product of two matrices, containing the useful signal and the noise terms respectively.

Consequently, the only form to derive an expression for the multidimensional speckle noise model is to transform the covariance matrix formulation to a vectorial formulation.

In Section 2.3.3 on page 42, the vectorization operator $V(\cdot)$ was introduced to transform the scattering matrix into the scattering vector $\mathbf{k}$. The same approach is employed now to transform the covariance $[C]$ and the sample covariance $[Z]$ matrices into vectorial forms. These vectorization process has to be performed taking into account the particularities of data which is being analyzed. In this case, the expression for the multidimensional speckle noise model will be obtained for PolSAR data in the backscattering case.

Let $\mathbb{C}^{3\times 3}$ be the space of 3×3 complex matrices. A vectorization of any 3×3 complex matrix can be introduced by considering an expansion of this matrix onto a set H of 9 3×3 complex matrices, provided H to be a complete set. Let $[M]$ be an arbitrary 3×3 complex matrix, it can be expressed as

$$[M] = \sum_{k=3p+q} m_k \eta_k \tag{5.97}$$

where the complex coefficients m_{3p+q} are obtained as

$$m_{3p+q} = \frac{1}{2}\mathrm{tr}([M]\eta_{3p+q}). \tag{5.98}$$

In this case, $\mathrm{tr}(\cdot)$ stands for the matrix trace. The coefficients p and q denote the row and column indexes of the matrix $[M]$, ranging from 0 to 2. In this case, interest is focused on the set H formed as the straightforward lexicographic ordering of the elements of $[M]$

$$\begin{aligned} H &= \{\eta_0,\eta_1,\eta_2,\eta_3,\eta_4,\eta_5,\eta_6,\eta_7,\eta_8\} \\ &= \left\{ \begin{bmatrix} 2&0&0\\0&0&0\\0&0&0 \end{bmatrix}, \begin{bmatrix} 0&2&0\\0&0&0\\0&0&0 \end{bmatrix}, \begin{bmatrix} 0&0&2\\0&0&0\\0&0&0 \end{bmatrix}, \right. \\ &\quad \begin{bmatrix} 0&0&0\\2&0&0\\0&0&0 \end{bmatrix}, \begin{bmatrix} 0&0&0\\0&2&0\\0&0&0 \end{bmatrix}, \begin{bmatrix} 0&0&0\\0&0&2\\0&0&0 \end{bmatrix}, \\ &\quad \left. \begin{bmatrix} 0&0&0\\0&0&0\\2&0&0 \end{bmatrix}, \begin{bmatrix} 0&0&0\\0&0&0\\0&2&0 \end{bmatrix}, \begin{bmatrix} 0&0&0\\0&0&0\\0&0&2 \end{bmatrix} \right\}. \end{aligned} \tag{5.99}$$

Consequently, the entries m_r of the vectorization of a 3×3 complex matrix $[M]$, i.e., $\mathbf{m} = [m_0, m_2, \ldots, m_8]^T$, are obtained as

$$m_r = \frac{1}{2}\mathrm{tr}([M]H_r) \tag{5.100}$$

for $r \in \{0,1,\ldots,8\}$. Instead of the orthonormal set H, the vectorization of the covariance $[C]$ and the sample covariance $[Z]$ matrices will be based on a different ordering

$$H_{ord} = \{\eta_0,\eta_4,\eta_8,\eta_1,\eta_2,\eta_3,\eta_5,\eta_6,\eta_7\}. \tag{5.101}$$

The new orthonormal base H_{ord} allows the diagonal elements of a given matrix to be located at the first positions of the derived vector. In the case of the sample covariance matrix $[Z]$, this fact facilitates the analysis, as the covariance matrix diagonal elements are affected only by a multiplicative speckle noise term.

Considering the expression for the Hermitian product speckle noise model, Eq. (5.95), the 3×3

complex covariance matrix $[C]$ can be divided into two new 3×3 complex matrices as follows

$$\begin{aligned}
[C] &= [C_1] + [C_2] \\
&= \begin{bmatrix} \psi_0 & \sqrt{2}\psi_1 N_{c_1}\overline{z}_{n_1} e^{j\phi_{x_1}} & \psi_2 N_{c_2}\overline{z}_{n_2} e^{j\phi_{x_2}} \\ \sqrt{2}\psi_3 N_{c_3}\overline{z}_{n_3} e^{j\phi_{x_3}} & 2\psi_4 & \sqrt{2}\psi_5 N_{c_5}\overline{z}_{n_5} e^{j\phi_{x_5}} \\ \psi_6 N_{c_6}\overline{z}_{n_6} e^{j\phi_{x_6}} & \sqrt{2}\psi_7 N_{c_7}\overline{z}_{n_7} e^{j\phi_{x_7}} & \psi_8 \end{bmatrix} \\
&+ \begin{bmatrix} 0 & \sqrt{2}\psi_1(|\rho_1| - N_{c_1}\overline{z}_{n_1}) e^{j\phi_{x_1}} & \psi_2(|\rho_2| - N_{c_2}\overline{z}_{n_2}) e^{j\phi_{x_2}} \\ \sqrt{2}\psi_3(|\rho_3| - N_{c_3}\overline{z}_{n_3}) e^{j\phi_{x_3}} & 0 & \sqrt{2}\psi_5(|\rho_5| - N_{c_5}\overline{z}_{n_5}) e^{j\phi_{x_5}} \\ \psi_6(|\rho_6| - N_{c_6}\overline{z}_{n_6}) e^{j\phi_{x_6}} & \sqrt{2}\psi_7(|\rho_7| - N_{c_7}\overline{z}_{n_7}) e^{j\phi_{x_7}} & 0 \end{bmatrix}
\end{aligned} \tag{5.102}$$

The factors 2 and $\sqrt{2}$ are required in order to keep the vector norm consistent with the span when the scattering matrix $[S]$ is considered as a three dimensional target vector $\mathbf{k}$ in the backscattering case. Since any covariance matrix is hermitian, the equalities: $|\rho_r| = |\rho_{r'}|$, $N_{c_r} = N_{c_{r'}}$, $\overline{z}_{n_r} = \overline{z}_{n_{r'}}$ and $\phi_{x_r} = -\phi_{x_{r'}}$ for the pairs of elements $[r, r'] = \{[1,3],[2,6],[5,7]\}$ apply. The vectorization operator given by Eq. (5.100) is employed with the orthonormal basis H_{ord} to derive the 9 complex entries of the vector forms of the matrices $[C_1]$, i.e., $\mathbf{c}_1$, and $[C_2]$, i.e., $\mathbf{c}_2$

$$c_{1,r} = \frac{1}{2}\mathrm{tr}([C_1]H_{ord,r}) \tag{5.103}$$

$$c_{2,r} = \frac{1}{2}\mathrm{tr}([C_2]H_{ord,r}) \tag{5.104}$$

for $r \in \{0, 1, \ldots, 8\}$. In the same way, the 9-dimensional vector form $\mathbf{z}$ of the sample covariance matrix $[Z]$, has its components defined as

$$z_r = \frac{1}{2}\mathrm{tr}([Z]H_{ord,r}) \tag{5.105}$$

for $r \in \{0, 1, \ldots, 8\}$. The covariance vector $\mathbf{c}$ represents the useful signal component contained in the sample covariance vector $\mathbf{z}$ which is damaged by the different speckle noise terms and has to be recovered. Since all the elements of the sample covariance vector consist in the Hermitian product of SAR images, which have been demonstrated to have the speckle noise model given by Eq. (5.95), the sample covariance vector can be written as

$$\mathbf{z} = [N_m]\mathbf{c}_1 + \mathbf{c}_2 + \mathbf{n}_a. \tag{5.106}$$

The matrix 9×9 real matrix $[N_m]$ contains the multiplicative speckle noise terms for all the elements of the covariance vector, whose expression is

$$[N_m] = \begin{bmatrix} n_{m_0} & 0 & 0 & 0 & 0 & 0 & 0 & 0 & 0 \\ 0 & n_{m_4} & 0 & 0 & 0 & 0 & 0 & 0 & 0 \\ 0 & 0 & n_{m_8} & 0 & 0 & 0 & 0 & 0 & 0 \\ 0 & 0 & 0 & n_{m_1} & 0 & 0 & 0 & 0 & 0 \\ 0 & 0 & 0 & 0 & n_{m_2} & 0 & 0 & 0 & 0 \\ 0 & 0 & 0 & 0 & 0 & n_{m_3} & 0 & 0 & 0 \\ 0 & 0 & 0 & 0 & 0 & 0 & n_{m_5} & 0 & 0 \\ 0 & 0 & 0 & 0 & 0 & 0 & 0 & n_{m_6} & 0 \\ 0 & 0 & 0 & 0 & 0 & 0 & 0 & 0 & n_{m_7} \end{bmatrix}. \tag{5.107}$$

On the contrary, the nine-dimensional complex vector $\mathbf{n}_a$ contains the additive speckle noise terms for the sample covariance vector components. Since the three first entries correspond to the diagonal elements of the sample covariance matrix $[Z]$, they equal zero as it has been demonstrated above. Hence, the vector

$\mathbf{n}_a$ is

$$\mathbf{n}_a = \begin{bmatrix} 0 \\ 0 \\ 0 \\ \psi_1(n_{ar_1} + jn_{ai_1}) \\ \psi_2(n_{ar_2} + jn_{ai_2}) \\ \psi_3(n_{ar_3} + jn_{ai_3}) \\ \psi_5(n_{ar_5} + jn_{ai_5}) \\ \psi_6(n_{ar_6} + jn_{ai_6}) \\ \psi_7(n_{ar_7} + jn_{ai_7}) \end{bmatrix}. \tag{5.108}$$

Eq. (5.106) represents the speckle noise model for PolSAR data, in the backscattering case, expressed under a covariance matrix formulation. In summary, this model represents a generalization of the multiplicative speckle noise model which applies for any SAR image intensity, allowing to identify the noise sources in the case of PolSAR data and how these noise sources damage the useful information which is contained on the data's correlation structure. The model presented by Eq. (5.106) can be conveniently extended to consider speckle noise effects for multidimensional SAR imagery, in which Q SAR images are considered under the covariance matrix formulation.

5.5 Validation and Interpretation

The present section is devoted to validate the multidimensional speckle noise model which has been proposed previously, with special attention to PolSAR data. This validation process will also serve to interpret the noise model, allowing to extract important conclusions about the speckle noise behavior for multidimensional SAR data. The validation, as well as the interpretation processes will be based on the analysis of the Hermitian product real and imaginary parts, whose speckle noise models are respectively given by Eqs. (5.93) and (5.94), instead to analyze directly the complex speckle noise model, Eq. (5.95). The results which will be extracted from this study can be easily extended to the covariance matrix speckle noise model introduced in Eq. (5.106). Additionally, since PolSAR is the perfect vehicle to validate the multidimensional speckle noise problem, real PolSAR data will be employed for this validation. Consequently, the products $S_{pq}S_{rs}^*$ where p, q, r and s refer to a pair of orthogonal polarization states, are considered. In this study the pair of horizontal and vertical polarization states $\{\widehat{\mathbf{h}}, \widehat{\mathbf{v}}\}$ is considered since most of the existing PolSAR systems work with this polarization basis.

Before to present to the study of the speckle noise model for the complex Hermitian product, Eq. (5.95), two definitions, referring to the different noise processes within this noise model, are introduced. The definitions

$$S_{pq}S_{rs}^* = \underbrace{\psi N_c \overline{z}_n n_m e^{j\phi_x}}_{Multiplicative\ term} + \underbrace{\psi(|\rho| - N_c\overline{z}_n)e^{j\phi_x} + \psi(n_{ar} + jn_{ai})}_{Additive\ term} \tag{5.109}$$

take into consideration the different speckle noise components. The first additive term of Eq. (5.109) will be simply referred as *Multiplicative term* since in this case, the useful signal is damaged by the multiplicative speckle noise component n_m. On the contrary, the second and the third additive terms are called the *Additive term* of the model since the second additive term, which contains useful signal, is damaged by the zero-mean speckle noise additive components of the third additive term, n_{ar} and n_{ai}. In Eq. (5.109) the terms $|\rho|$, N_c, $\overline{z}_n$ and ϕ_x refer to the joint properties of the SAR images S_{pq} and S_{rs}.

5.5.1 Hermitian Product Speckle Noise Model Validation: Simulated PolSAR Data

In the same way as it has been presented in Section 4.2.3 for the interferometric phasor noise model, the Hermitian product speckle noise model is validated first by means of simulated PolSAR data. These

data are obtained with the algorithm detailed in Section 4.2.3. In this case, the input parameters are the complex correlation coefficient ρ and the powers σ_{pq} and σ_{rs} of each one of the SAR images.

The first parameter in which the Hermitian product speckle noise model depends on is the average power term ψ, which equals $\sqrt{\sigma_{pq}\sigma_{rs}}$. As it can be concluded from the speckle noise model expression, Eq. (5.95), it only acts as an scaling parameter which does not affect the speckle noise final nature. Consequently, without loss of generality, unit power SAR images can be considered, i.e., $\psi = 1$.

The coherence parameter $|\rho|$ has a direct impact on the final nature of speckle noise for the Hermitian product real and imaginary parts, since the standard deviations of the zero-mean additive speckle noise terms, n_{ar} and n_{ai}, depend directly on it, see Eq. (5.92). On the contrary, the standard deviation of the multiplicative speckle noise term n_m is constant and equal to one for the whole coherence range. If instead of considering the multiplicative speckle noise component n_m, the complete multiplicative term of the Hermitian product speckle noise model, as defined in Eq. (5.109), is considered, it can be observed that the standard deviation of this term depends on the coherence value through the parameter N_c. The type of dependence, regardless of the phase value ϕ_x, is directly proportional to the coherence value $|\rho|$. Eq. (5.35) gives the actual value of the variance for the Hermitian product real part, whereas the approximated value can be derived from Eq. (5.36). Fig. 5.3 presents a graphical representation of these values. Hence, the multiplicative term presents low standard deviation values for low coherences and high ones for high coherences. As a brief summary, in the case of the Hermitian product real part, considering $\phi_x = 0$ rad, it can be concluded that the multiplicative term of the speckle noise model will be dominant, in terms of standard deviation, for high coherences, whereas the additive term is dominant for low coherences. The importance of the multiplicative term with respect to the additive one, in terms of standard deviation, is considered by means of the equality

$$N_c \overline{z}_n \sigma_{n_m} = \sigma_{n_{ar}} = \sigma_{n_{ai}}. \tag{5.110}$$

This equality becomes true for $|\rho| = 0.675$. Therefore, the additive speckle noise terms, n_{ar} and n_{ai}, are dominant for the majority of the coherence values, being the multiplicative term dominant only for coherences higher than 0.675. As a result, the speckle noise in the case of the Hermitian product real and the imaginary parts is clearly dominated, for medium and low coherences, by an additive noise behavior, regardless of the phase value ϕ_x. Above this value, the speckle noise is dominated by a multiplicative behavior.

In the previous paragraph, the effect of the terms $\cos(\phi_x)$ and $\sin(\phi_x)$ has not been considered. As demonstrated, none of the noise terms n_m, n_{ar} neither n_{ai} present a direct dependence on it. Nevertheless, the final nature of the speckle noise for the real and imaginary parts of the Hermitian product depends indirectly on $\cos(\phi_x)$ and $\sin(\phi_x)$, respectively. The clear effect of these terms can be observed over the standard deviation value of the multiplicative term, which equals $N_c \overline{z}_n \sigma_{n_m} \cos(\phi_x)$ in the Hermitian product real part case and $N_c \overline{z}_n \sigma_{n_m} \sin(\phi_x)$ in the Hermitian product imaginary part case. The terms $\cos(\phi_x)$ and $\sin(\phi_x)$ also affect the deterministic component of the additive term, but not the additive noise terms n_{ar} and n_{ai}. Retaking what has been explained in the previous paragraph, the standard deviation of the multiplicative term is controlled, on the one hand, by the parameter N_c, and, on the other hand, by the terms $\cos(\phi_x)$ and $\sin(\phi_x)$ for the real and imaginary part cases, respectively. Thus, the relative importance of the multiplicative term given in Eq. (5.109), in terms of standard deviation, depends on the terms $N_c \cos(\phi_x)$ and $N_c \sin(\phi_x)$ for the Hermitian product real and imaginary parts. The main consequence of this dependence is that the final nature of speckle noise will be different for the real and imaginary parts of the complex Hermitian product.

Before to present the validation process in the case of simulated SAR data, it is necessary to determine the form in which the multiplicative and the additive terms in Eq. (5.109) are obtained. As it has been presented, the multiplicative term of the speckle noise model consists of the product of the Hermitian product amplitude z by the term $N_c \exp(j\phi_x)$. This term can be obtained from the complex correlation coefficient ρ, since the parameter N_c is a function of $|\rho|$, see Eq. (4.11), and the phase ϕ_x corresponds

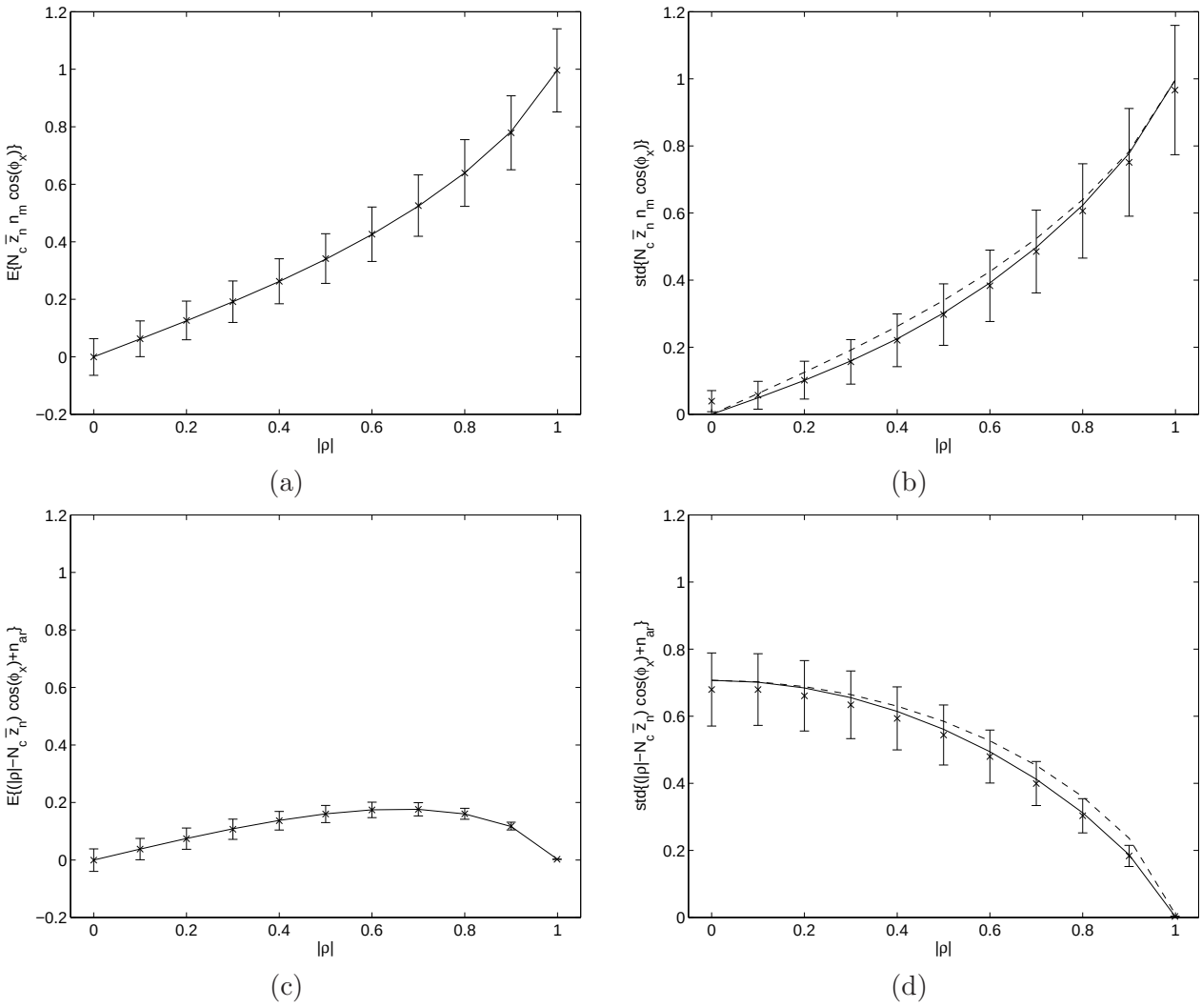

Figure 5.12: Monte-Carlo analysis to test the validity of the speckle noise model for the real part of the Hermitian product of a pair of SAR images. (a) Mean value for the multiplicative term. (b) Standard deviation for the multiplicative term. (c) Mean value for the additive term. (d) Standard deviation for the additive term. Solid lines represent theoretical values as a function of $|\rho|$, whereas dashed lines represent the approximated values. Crosses represent the estimated values. In all the cases $\phi_x = 0$ rad and $\psi = 1$.

to the phase of ρ. The additive term is, therefore, obtained as the difference between the total complex Hermitian product and the multiplicative term, obtained as explained above.

The validation process of the speckle noise model, given by Eq. (5.95), has consisted on comparing the mean and the standard deviation values estimated from simulated data, obtained by means of the usual sample estimators, with those predicted by the theoretical model. In all the cases, the statistical values, as well as the different model parameters, are obtained by means of 7 by 7 pixel, non-overlapped windows over 512 by 512 pixel simulated SAR images. The first test has consisted of simulating SAR images for the whole coherence range, for the particular average phase difference of $\phi_x = 0$ rad. Figs. 5.12 and 5.13 present the results of this series of simulated SAR data for the real and imaginary parts of the Hermitian product, respectively. The standard deviation corresponding to the estimators is also presented as the graphic bars.

As it can be deduced from Figs. 5.12 and 5.13, it exists a complete agreement between the values of the different statistical moments corresponding to the different components of the speckle noise model derived from simulated data and the theoretical values predicted by the model. A complete agreement is observed in the case of the mean values, whereas minor differences can be noticed in the case of the standard deviations, as a consequence of the approximations which have been introduced and the

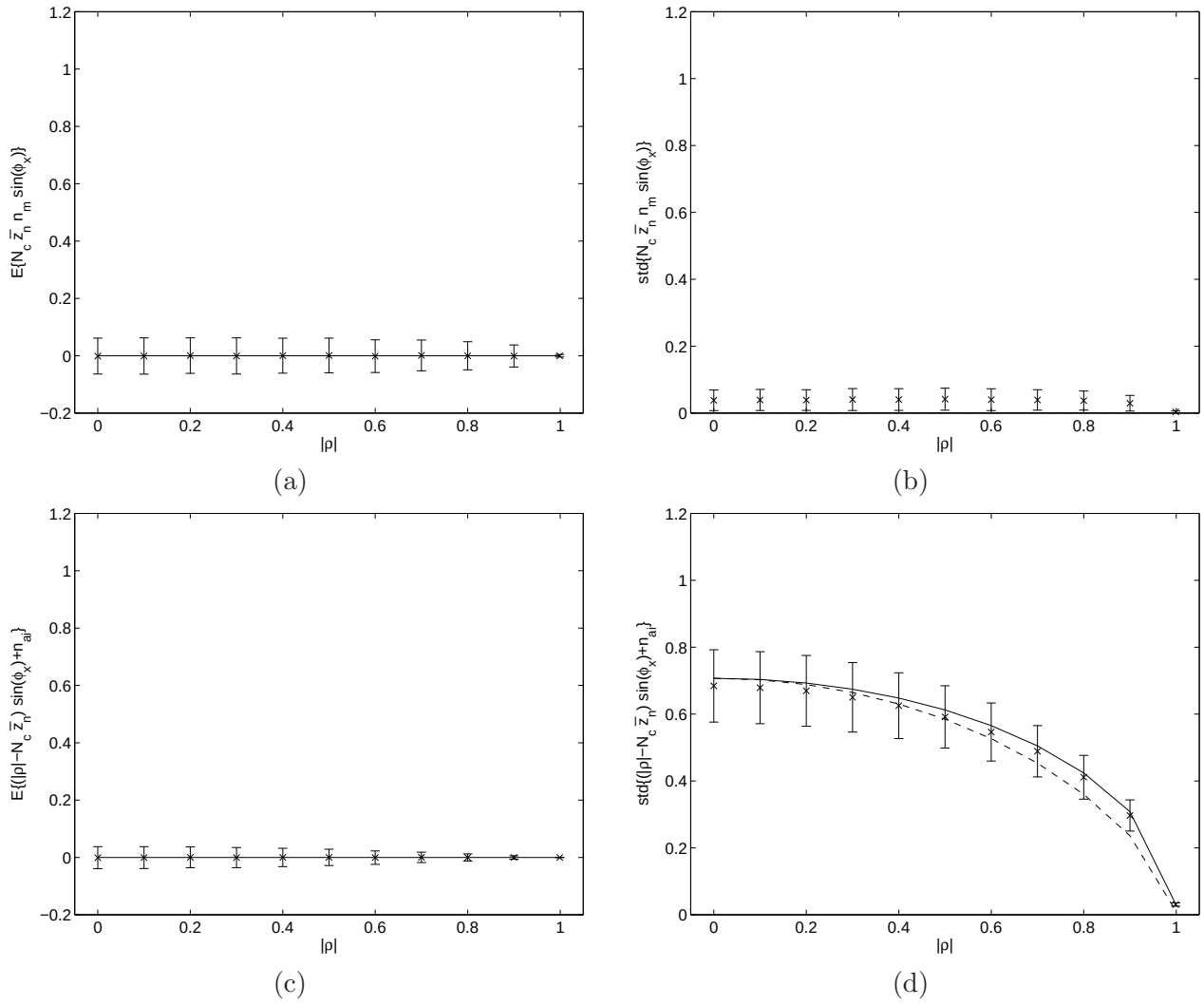

Figure 5.13: Monte-Carlo analysis to test the validity of the speckle noise model for the imaginary part of the Hermitian product of a pair of SAR images. (a) Mean value for the multiplicative term. (b) Standard deviation for the multiplicative term. (c) Mean value for the additive term. (d) Standard deviation for the additive term. Solid lines represent theoretical values as a function of $|\rho|$, whereas dashed lines represent the approximated values. Crosses represent the estimated values. In all the cases $\phi_x = 0$ rad and $\psi = 1$.

insufficient number of samples employed for the estimation. These minor differences disappear if larger windows, as for instance 11 by 11 pixel, non-overlapped windows, are employed. From Fig. 5.12b, it can be observed that the standard deviation of the multiplicative term, in the real part case, is proportional to the coherence value $|\rho|$, whereas from Figs. 5.12d and 5.13d one observes that the additive components have an inverse dependence on $|\rho|$. Additionally, if Fig. 5.12 is compared with 5.13, one can observe the indirect dependence on the phase ϕ_x, in this case for $\phi_x = 0$ rad. Whereas the Hermitian product real part presents both, multiplicative and additive speckle noise terms, the imaginary part is only affected by the additive speckle noise term n_{ai}, for any coherence value. Finally, Fig. 5.14 presents the values obtained for the covariance term $\mathcal{C}_{12}$. In this case, the agreement between the theoretical and the values estimated from simulated data can also be observed.

The indirect effect of the true phase difference ϕ_x has been also tested with simulated SAR images in which the coherence value remains constant and equal to $|\rho| = 0.675$, and the phase ϕ_x varies from 0 rad to π rad. Fig. 5.15 presents the results of the Monte-Carlo analysis for the standard deviation values.

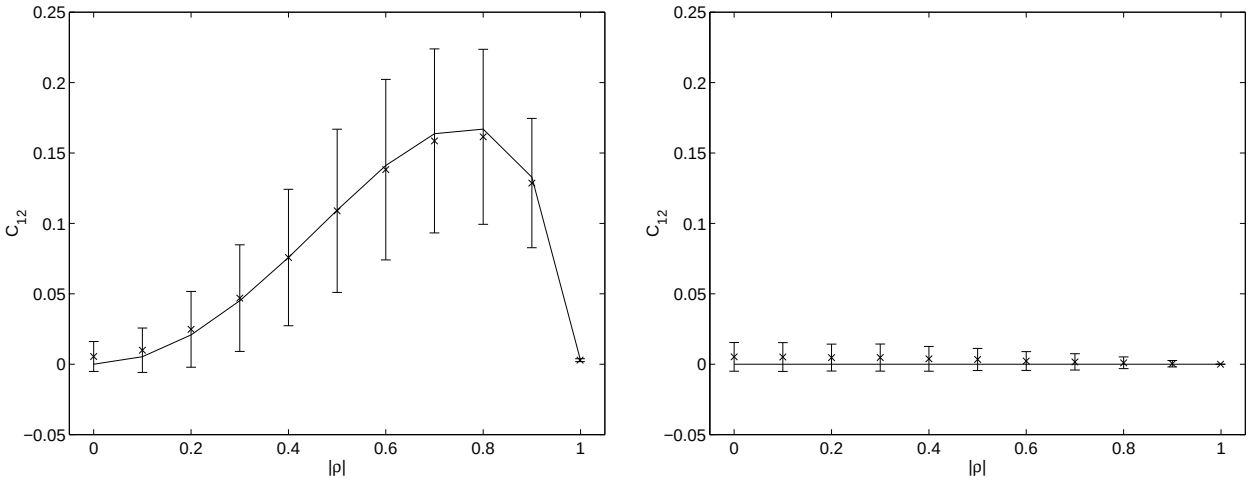

Figure 5.14: Monte-Carlo analysis to test the parameter $\mathcal{C}_{12}$ for the Hermitian product. (a) Real part. (b) Imaginary part. Solid lines represent theoretical values. Crosses represent the estimated values. In all the cases $\phi_x = 0$ rad and $\psi = 1$.

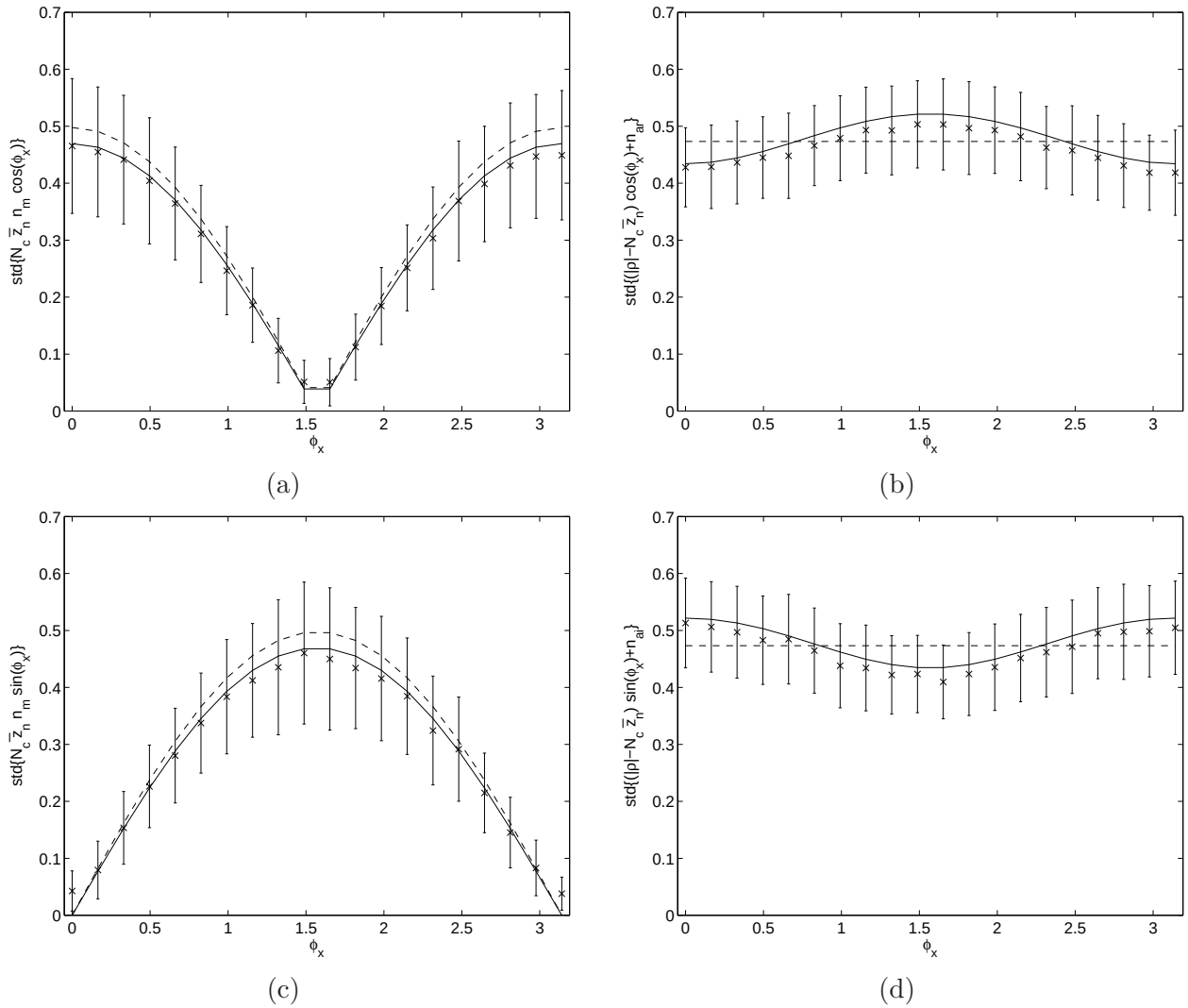

Figure 5.15: Monte-Carlo analysis to test the speckle noise model for the Hermitian product. (a) Standard deviation value for the multiplicative component of the real part. (b) Standard deviation value for the additive component of the real part. (c) Standard deviation value for the multiplicative component of the imaginary part. (d) Standard deviation value for the additive component of the imaginary part. Solid lines represent theoretical values as a function of $|\rho|$, whereas, dashed lines represent the approximated values. Crosses represent estimated values. In all the cases $|\rho| = 0.675$ rad and $\psi = 1$.

From this figure, one observes which is the final nature of the Hermitian product speckle noise. As it can be observed in Figs. 5.15b and 5.15d, the standard deviation of the zero-mean, additive noise terms n_{ar} and n_{ai} have a small dependence on the phase difference ϕ_x, which is eliminated in the approximated values as explained in Section 5.4.5. On the contrary, the final standard deviation of the multiplicative term in the real and imaginary parts of the Hermitian product have a clear dependence on the phase ϕ_x. It can be concluded, therefore, that the final nature of speckle noise for the real and imaginary parts of the Hermitian product depends, both, on the coherence $|\rho|$ and on the phase ϕ_x. But, since the multiplicative term of the Hermitian product real part depends on $\cos(\phi_x)$ and the imaginary one depends on $\sin(\phi_x)$, the real and imaginary parts of the Hermitian product present speckle noises with different natures. For instance, for $\phi_x = 0$ rad, the Hermitian product real part contains multiplicative as well as additive speckle, since the corresponding standard deviation values are different from zero. On the contrary, the imaginary part only contains additive speckle. For $\phi_x = \pi/2$ rad, the opposite situation is produced, since the imaginary part of the Hermitian product presents multiplicative as well as additive speckle, whereas the real part of the Hermitian product presents only additive speckle noise. It can be concluded that the final importance (or weight) of the multiplicative speckle term in the Hermitian product depends basically on the term $N_c \exp(j\phi_x)$, whereas the importance of the additive terms n_{ar} and n_{ai} depend only on $|\rho|$.

5.5.2 Hermitian Product Speckle Noise Model Validation: Real PolSAR Data

The speckle noise model for the complex Hermitian product of a pair of SAR images will be now validated by means of real PolSAR data. This model has been derived for a general Hermitian product without making any assumption concerning the information content or introducing any restriction. Consequently, the validity of the Hermitian product speckle noise model for PolSAR data can be proven, without loss of generality, analyzing only one covariance matrix entry, and analyzing the results to the rest of covariance matrix entries. The data employed in this section correspond to an 1321 by 14654 pixel, L-band (1.3 GHz), fully polarimetric dataset acquired by the E-SAR system [185] over the Oberpfaffenhofen area, nearby the German city of Munich, on the summer of 2001. The data was acquired in the linear polarization basis $\{\widehat{\mathbf{h}}, \widehat{\mathbf{v}}\}$ and processed by the DLR-HR. The proposed speckle noise model will be tested on the covariance matrix off-diagonal element $S_{hh}S_{vv}^*$. As previously demonstrated, the final speckle noise nature depends on the complex correlation coefficient between the SAR images S_{hh} and S_{vv}. Fig. 5.16 presents the complex correlation coefficient calculated by means of 7 by 7 pixel, non-overlapped, windows.

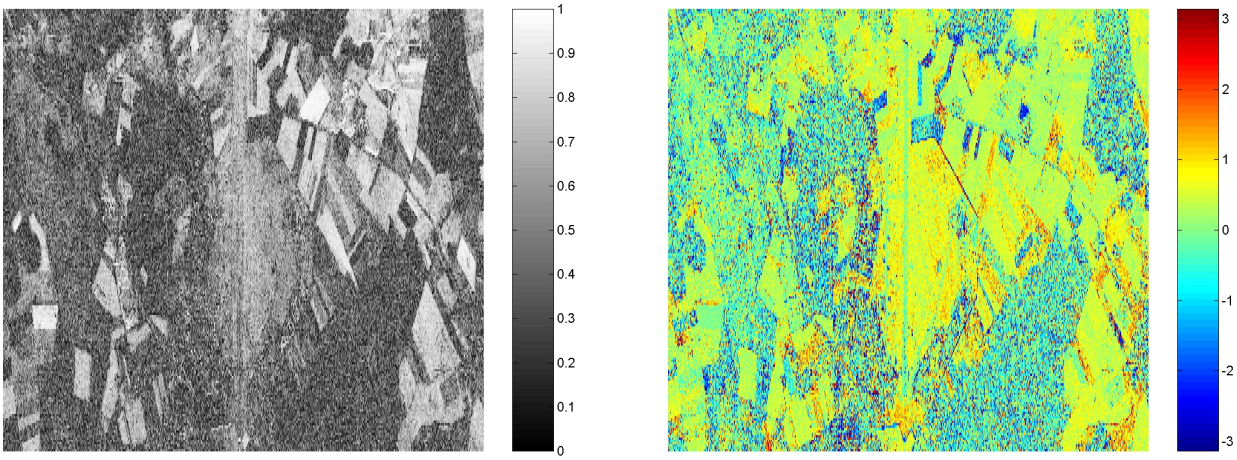

(a) (b)

Figure 5.16: Oberpfaffenhofen test site. Complex correlation coefficient ρ corresponding to the covariance matrix element $S_{hh}S_{vv}^*$. (a) Amplitude $|\rho|$. (b) Phase ϕ_x (rad).

As it can be deduced from Fig. 5.16, the complex correlation coefficient amplitude and the phase are non homogeneous across the image. The first important consequence is that the speckle noise nature will not be homogeneous, ranging hence, from areas with a complete multiplicative speckle to areas where it is fully additive.

The Oberpfaffenhofen dataset is analyzed in two different ways. On the one hand, the dataset will be considered globally through the calculation of mean versus standard deviation scatter diagrams [1]. On the other hand, the dataset is examined locally. This analysis consists, as it has been performed previously, in comparing statistical moments obtained from real data with the corresponding theoretical values. In this case two homogeneous areas characterized by a high and a low coherence values will be considered.

Scatter diagrams in which the standard deviation value is presented as a function of the mean value are valuable as they offer information concerning the noise processes under study [1]. Fig. 5.17 presents the scatter diagram for the Hermitian product real part $\Re\{S_{hh}S_{vv}^{*}\}$, where the color codes density, i.e., blue for low and red for high densities, respectively. In this case, the mean and the standard deviation values have been calculated with the usual sample estimators over 7 by 7 pixel, non-overlapped windows. As it can be observed from this diagram, it is not possible to derive any conclusion about the speckle noise nature. Nevertheless, it can be noticed that it exists a validity region limited by the lines with slopes 1 and -1 which cross the axis origin. As it has been noticed in the previous section, regardless the phase dependence, in the case of the Hermitian product real and imaginary parts, the speckle noise is dominated by a multiplicative behavior for high coherences whereas the dominant mechanism is additive for low coherences. Fig. 5.18 presents the scatter diagram given at Fig. 5.16, but divided for different coherence $|\rho|$ ranges. In each case, the multiplicative and the additive terms, as presented by Eq. (5.109), are also given. Fig. 5.18 makes evident the speckle behavior for the different coherence values. If the second column is observed, one can notice that the larger the coherence value, the most important the multiplicative component. In this case, two branches, over the lines of slope 1 and -1 are observed, since the multiplicative term mean value can be either positive or negative. This behavior is given, in this case, by the sign of $\cos(\phi_x)$. For the imaginary part case, the sign will be given by $\sin(\phi_x)$. If one now observes the third column, corresponding to the additive term of $\Re\{S_{hh}S_{vv}^{*}\}$, it can be concluded that the lower the coherence value, the most important the additive component. As it has been demonstrated in Section 5.4.2, as well as in Section 5.4.5, this term is characterized by an small mean value (lower than the 20% of the total signal) which depends on $|\rho|$ and a standard deviation which also depends inversely on $|\rho|$. Finally, if the first column of Fig. 5.18 is analyzed, it can be observed that the scatterer diagram is dominated by an additive behavior for low coherences, whereas it is almost multiplicative for high coherences. An important aspect that Fig. 5.18 points out is the importance of the speckle additive component. As it is evident from the third column of Fig. 5.18, the additive speckle term is significant even for coherences larger than 0.8. As a result, this additive component has to be carefully considered when speckle is eliminated.

The behavior of the scatter diagrams corresponding to the Hermitian product imaginary part $\Im\{S_{hh}S_{vv}^{*}\}$ is completely parallel to the one shown in Fig. 5.18. The only difference in this case is that the scatter diagrams vary according to $\sin(\phi_x)$ instead to $\cos(\phi_x)$.

The aim of the following part of this section is to present a quantitative validation of the Hermitian product speckle noise model, Eq. (5.95), employing real data. This test consists in comparing the moments of the multiplicative and the additive terms of the speckle noise model for the real and imaginary parts of the Hermitian product with the values given by the theoretical model. The procedure employed to divide and to analyze the signal is the same one employed previously to analyze simulated data, which consists in estimating the different moments over 7 by 7 non-overlapped windows. In this case, data has been normalized by its corresponding power ψ, since this factor only acts as a scaling term on the speckle noise model for the Hermitian product. The test has been applied over two different areas of the Oberpfaffenhofen test site. The fist area is characterized by a high coherence value, whose complex

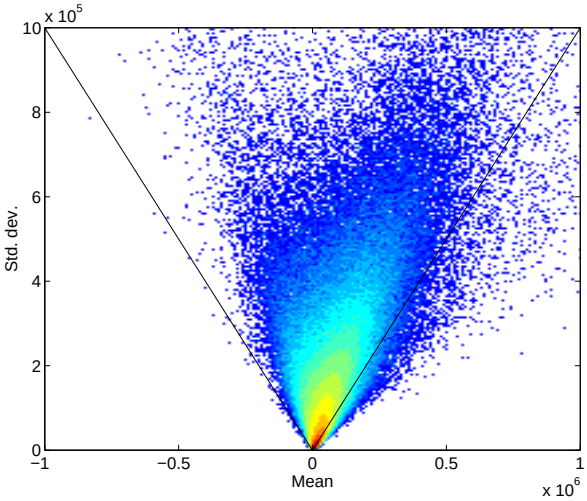

Figure 5.17: Global scatter diagram for $\Re\{S_{hh}S_{vv}^*\}$ in the case of the Oberpfaffenhofen test site.

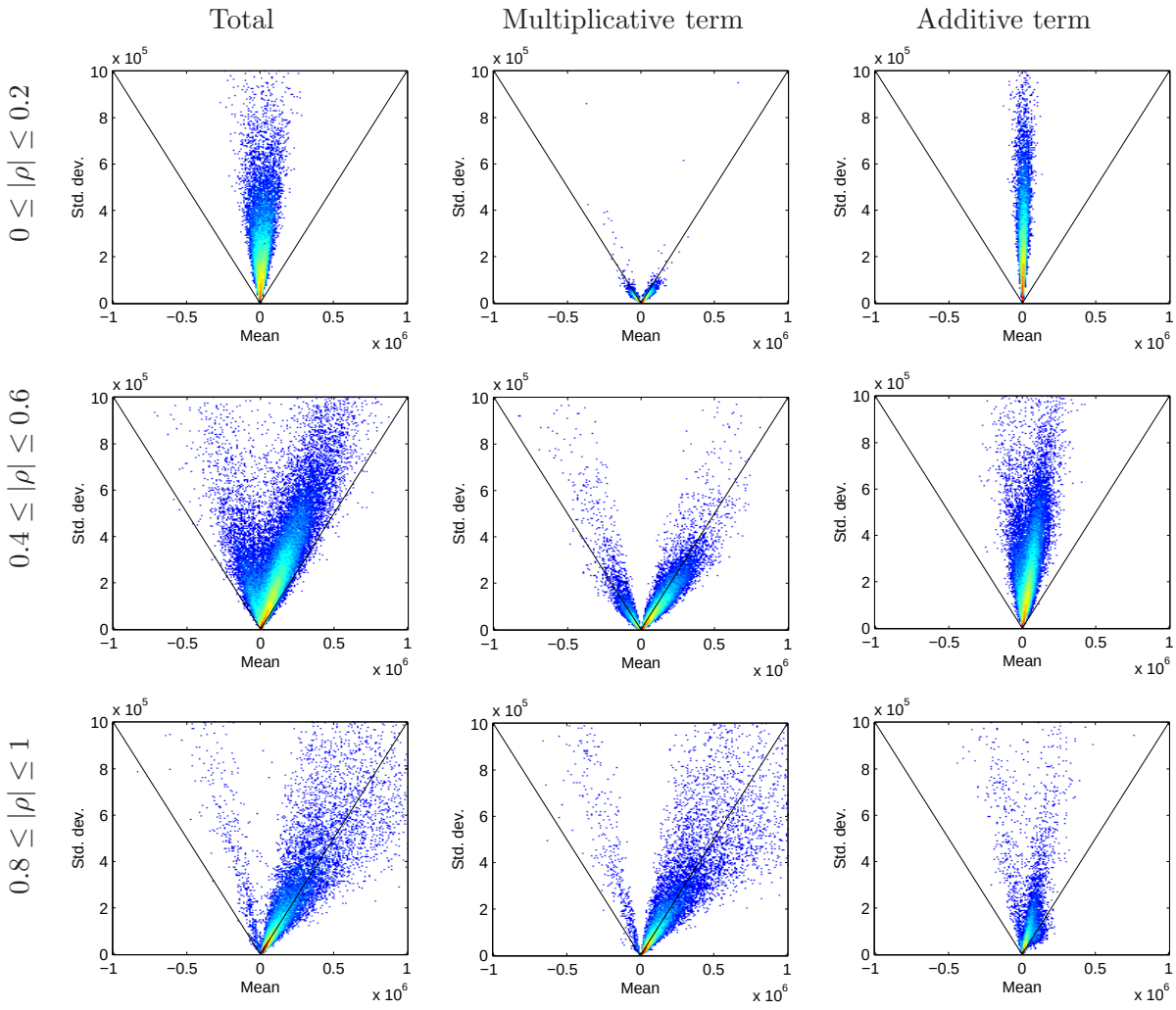

Figure 5.18: Scatter diagrams for $\Re\{S_{hh}S_{vv}^*\}$ in the case of the Oberfapfenhoffen test site.

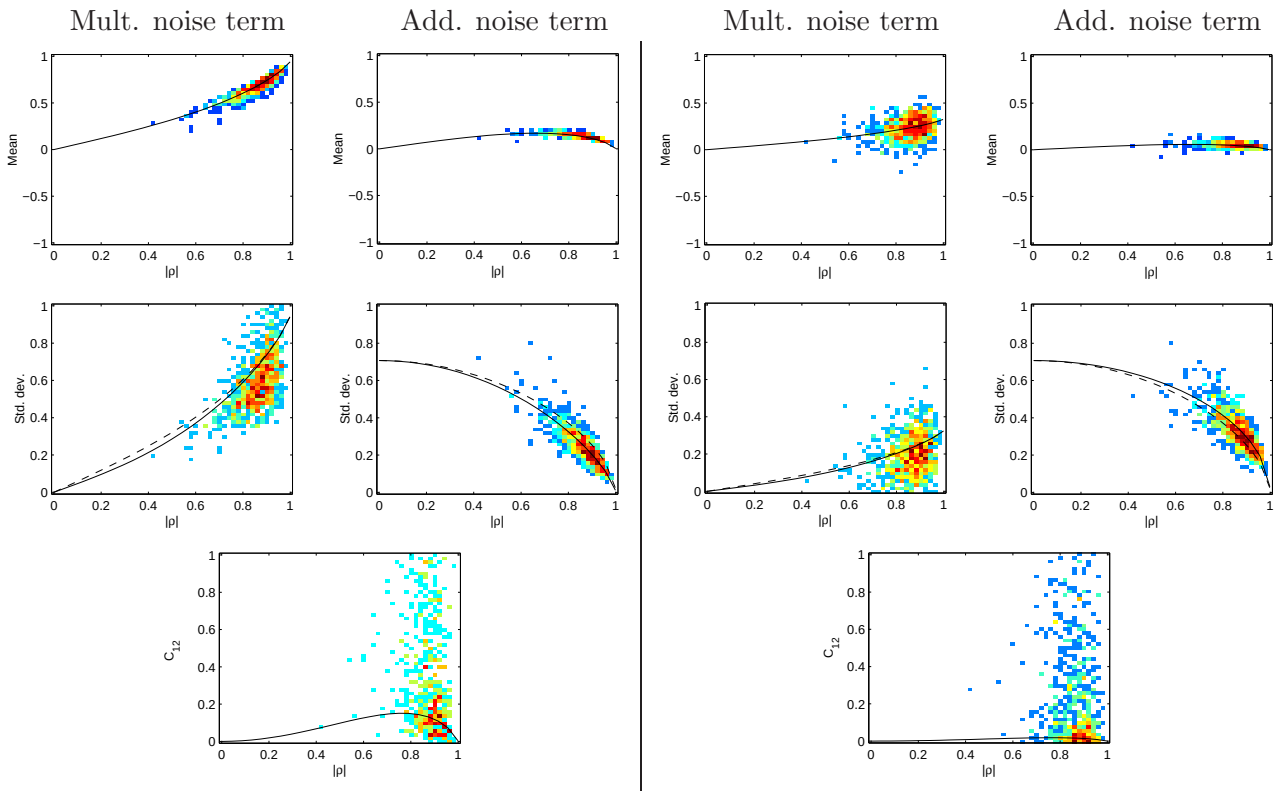

(a) $\Re\{S_{hh}S_{vv}^*\}$ (b) $\Im\{S_{hh}S_{vv}^*\}$

Figure 5.19: Comparison between real and theoretical values for the different components of the speckle noise model for a high coherence area, $\rho = 0.850\exp(j0.331)$. (a) Hermitian product real part $\Re\{S_{hh}S_{vv}^*\}$. (b) Hermitian product imaginary part $\Im\{S_{hh}S_{vv}^*\}$. Solid and dashed lines represent actual and approximated values respectively. Points indicate data statistics where color refers to density, ranging from low densities (blue) to high densities (red).

		a$_0$	a$_1$	s	r
$\Re\{S_{hh}S_{vv}^*\}$	Mean mult.	0	0.994	0.011	0.994
	Std. mult.	0.043	0.842	0.121	0.597
	Mean add.	0.007	0.971	0.011	0.921
	Std. add.	-0.068	1.041	0.051	0.846
	C$_{12}$	-1.603	29.668	4.409	0.158
$\Im\{S_{hh}S_{vv}^*\}$	Mean mult.	0	0.993	0.004	0.998
	Std. mult.	0.003	0.896	0.045	0.894
	Mean add.	0	1.033	0.004	0.986
	Std add.	0.035	0.975	0.063	0.766
	C$_{12}$	0.824	6.575	2.566	0.044

(a)

		a$_0$	a$_1$	s	r
$\Re\{S_{hh}S_{vv}^*\}$	Mean mult.	0	0.990	0.011	0.996
	Std. mult.	0.001	0.868	0.034	0.938
	Mean add.	0	1.022	0.011	0.987
	Std. add.	-0.017	0.972	0.105	0.507
	C$_{12}$	0.079	0.311	0.157	0.077
$\Im\{S_{hh}S_{vv}^*\}$	Mean mult.	0	0.990	0.010	0.997
	Std. mult.	0.001	0.870	0.030	0.951
	Mean add.	0	1.020	0.010	0.989
	Std add.	-0.046	1.031	0.106	0.523
	C$_{12}$	0.019	1.358	0.065	0.614

(b)

Table 5.2: Least squares regression analysis results for the Oberfaphenhoffen test site. (a) Analysis corresponding to the high coherence area, whose complex coherence equals $0.850\exp(j0.331)$.(b) Analysis corresponding to the low coherence area, whose complex coherence equals $0.389\exp(j0.528)$.

correlation coefficient ρ equals $0.850\exp(j0.331)$. The second area is characterized by a low coherence, that is $\rho = 0.389\exp(-j0.528)$. Figs. 5.19 and 5.20 present the qualitative result of this comparison. As it can be observed in all the plots of these figures, a full agreement exists between the theoretical expressions, given by solid and dotted lines, and the values derived from real data. The levels of agreement between the theoretical and the calculated moments from data is independent of the Hermitian product real and imaginary parts or the degree of coherence between the pair of SAR images.

The level of agreement between theory and data has been also quantitatively measured by means

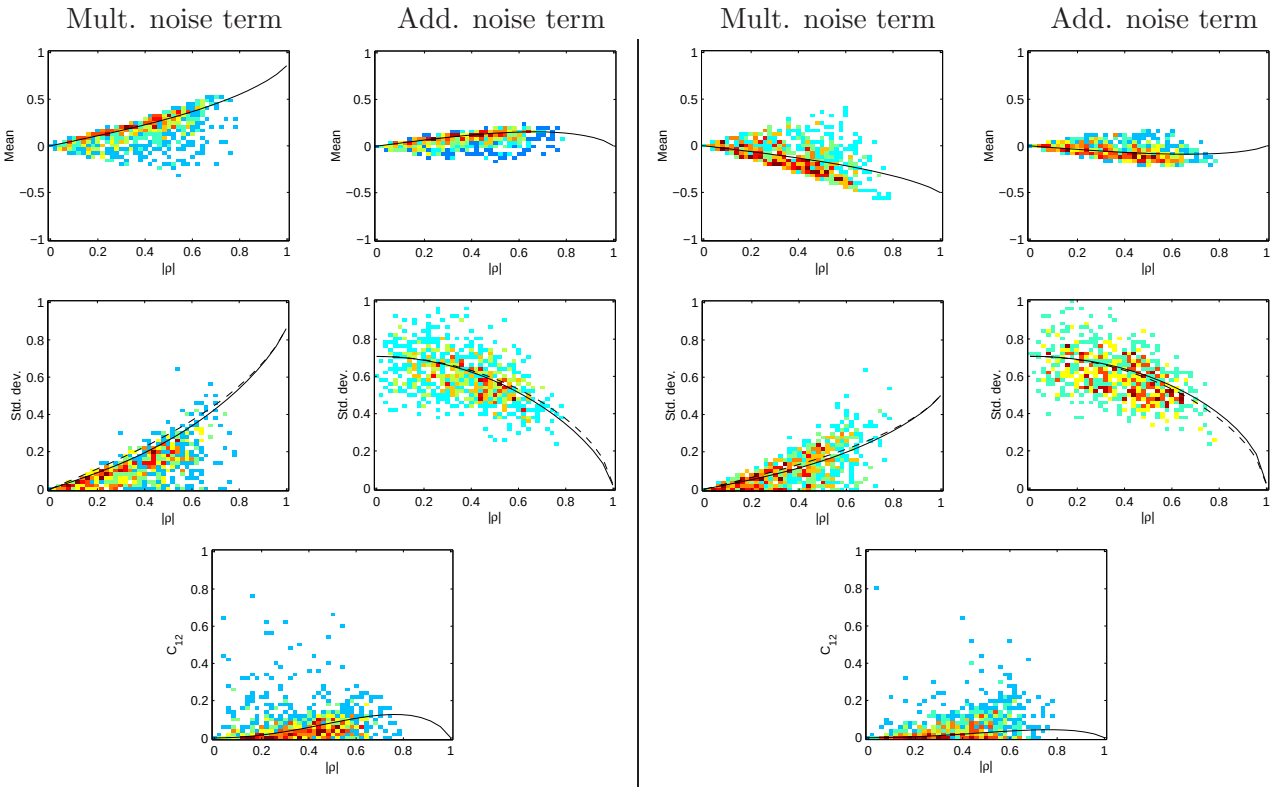

(a) $\Re\{S_{hh}S_{vv}^*\}$ (b) $\Im\{S_{hh}S_{vv}^*\}$

Figure 5.20: Comparison between real and theoretical values for the different components of the speckle noise model for a low coherence area, $\rho = 0.389\exp(-j0.528)$. (a) Hermitian product real part $\Re\{S_{hh}S_{vv}^*\}$. (b) Hermitian product imaginary part $\Im\{S_{hh}S_{vv}^*\}$. Solid and dashed lines represent actual and approximated values respectively. Points indicate data statistics where color refers to density, ranging from low densities (blue) to high densities (red).

of the same type of least squares regression analysis employed to validate the interferometric phasor noise model in the previous chapter. This analysis consists in calculating the regression curves between the theoretical values of the moments, obtained from the coherence calculated over data, and the same statistical values extracted from data. Tables 5.2a and 5.2b present the results of this analysis for all the plots shown in Figs. 5.19 and 5.20, respectively. The interpretation of the different parameters presented in these tables is found in Appendix D. The results obtained from the least squares regression analysis confirms the full agreement between the theoretical and the calculated values of the moments of the different components of the speckle noise model for the Hermitian product. The major agreement is obtained in the case of the mean values, which precisely contain the useful information which has to be maintained. The least squares regression analysis in the case of the standard deviation values has been performed considering the approximated values (dashed lines). Despite these approximations, the closeness between the theory and data is still very high. On the contrary, a major disagreement is obtained in the case of the covariance values $\mathcal{C}_{12}$. A quick look to the corresponding plots in Figs. 5.19 and 5.20 shows this disagreement, but also that the major density (red color) corresponds to the values over the theoretical curves. This disagreement is consequence of the insufficient number of data samples employed to calculate the covariance values $\mathcal{C}_{12}$. Figs. 5.19 and 5.20, corresponding to real data, make evident several points already observed in the simulated data case. Considering the standard deviation values corresponding to the high coherence area, Fig. 5.19, if one compares the values corresponding to the real part, Fig. 5.19a, with the corresponding to the imaginary one, Fig. 5.19b, it can be deduced that the real part is dominated by a multiplicative speckle behavior, whereas the imaginary part, despite the high coherence value, is dominated by an additive speckle noise behavior. On the contrary, if one makes the same comparison in the low coherence area, Fig. 5.20, it can be concluded that both, the

real and imaginary parts of the Hermitian product, are dominated by an additive speckle noise behavior, as a consequence of the low coherence value. These results over real data confirms that the speckle noise nature is not homogeneous in the image and that, even, this nature changes from the real to the imaginary part of the Hermitian product.

In this section, the speckle noise model has been validated for data obtained with respect to the linear polarization basis $\{\widehat{\mathbf{h}}, \widehat{\mathbf{v}}\}$. In Section 2.3.7 it was shown that given the scattering matrix measured in a given polarization basis, for instance the linear polarization basis $\{\widehat{\mathbf{h}}, \widehat{\mathbf{v}}\}$, it is possible to derive the scattering matrix in any other polarization basis. This change of basis will introduce also a change on the covariance matrix $[C]$, altering the data's correlation structure. This transformation will not change the speckle noise model itself, Eq. (5.106), as the complex Wishart pdf is maintained. But, since the correlation structure is altered, the nature of the speckle noise for each entry of the single-look covariance matrix $[Z]$ will vary according to the new correlation structure between the SAR images.

5.5.3 Hermitian Product Speckle Noise Model Validation: Extended Validation

The development of the proposed speckle noise model for the Hermitian product is based on the analysis of the scattering theory from an statistical perspective, and not on an experimental curve-fitting process. This procedure ensures that, whenever the conditions in which the model is based on are valid, data will follow the proposed speckle noise model. This reasoning explains the high level of agreement which has been obtained in the previous sections between theory and data.

The previous two sections have served to validate the proposed speckle noise model by means of simulated and real PolSAR data. These two cases, and in particular the latter, represent only a small portion of the wide range of conditions in which multidimensional, and in particular PolSAR data can be acquired. In addition to the analysis presented in the previous section, additional validation tests have been performed with different PolSAR datasets. The inclusion of the results of these analyses in this text will imply basically to repeat what has been already presented in Section 5.5.2. References concerning these additional analyses are provided.

The complex Hermitian product speckle noise model has been also tested with PolSAR data acquired with a spaceborne SAR sensor. In this case, experimental data correspond to a single-look, L-band (1.27 GHz), polarimetric dataset in the basis $\{\widehat{\mathbf{h}}, \widehat{\mathbf{v}}\}$. The data were acquired on autumn 1994 by the SIR-C/X-SAR radar system, processed by NASA/JPL and correspond to the southeastern edge of Baikal Lake, at the confluence of the Selenga stream, in Buriaria, Russia. Data consist in a 40 km azimuth by 20 km range image of agricultural and forestry areas. The results of this validation process were presented at the International Geoscience and Remote Sensing Symposium (IGARSS'02) held in Toronto, Canada on July 2002 [183]. The fist part of the analysis presented in this work consisted of studying the Hermitian product speckle noise model validity over the spaceborne PolSAR system dataset. The main result of the work was that the proposed speckle noise model was completely valid, also for data acquired from spaceborne platforms. The level of agreement between theory and data was very similar to the one presented in the previous section.

Most of the existing SAR sensors, placed either in airborne or spaceborne platforms, operate in a wide range of frequencies. Among other considerations, the frequency in which PolSAR data are acquired has two main consequences concerning the validity of the Hermitian product speckle noise model. On the one hand, the correlation properties between two SAR images of the same area depend on frequency. Consequently, the speckle noise nature will vary from one frequency to another accordingly to these correlation properties. On the other hand, the frequency in which the system operates has an indirect effect concerning the validity of the Hermitian product speckle noise model, since the resolution cell dimensions depend on the system parameters at each frequency. The Hermitian product speckle noise model is based on the Gaussian scattering assumption, which at the same time is concerned with the number of scatterers inside the resolution cell. Section 5.7 will be focused on presenting a multi-frequency

validation of the Hermitian product speckle noise model, allowing to extend the proposed speckle noise model to consider SAR images taken at different frequencies.

5.6 Polarimetric SAR Interferometric Speckle Noise Model

One of the results of Chapter 4 has been the definition of a noise model for the Hermitian product phase complex phasor in the frame of SAR interferometry. This noise model was taken as a basis to construct the speckle noise model for the Hermitian product of a pair of SAR images, which has been studied in Section 5.4.5. Finally, this model has made possible the definition of a vectorial speckle noise model for multidimensional SAR data, which has been validated in the frame of PolSAR. In the Section 2.4 at Chapter 2, it was shown that it is possible to combine InSAR and PolSAR data, through the concept of vector interferometry, as a way to investigate the vertical structure of a given scatterer. This technique is known as Polarimetric SAR Interferometry, shorten PolInSAR. One of the most promising applications of these data is the possibility to retrieve the vegetation's height information, since the availability of this parameter makes possible to estimate the quantity of Biomass. The main advantage of this technique, compared with techniques based on non coherent data, is that PolInSAR does not present saturation problems for a given amount of biomass.

PolInSAR data acquisition is based on measuring the complete scattering matrix $[S]$, for a given scatterer, from two slightly different positions in space. In the following, it will be assumed that the $[S]$ matrices are referred to the linear polarization basis $\{\widehat{\mathbf{h}}, \widehat{\mathbf{v}}\}$. Consequently, PolInSAR data will be affected also by speckle noise. As it has been mentioned previously, distributed scatterers can not be completely characterized by the scattering matrix measurements directly. Hence, this characterization has to be done over higher moments. In the backscattering case, each fully polarimetric data acquisition is determined by the corresponding three-dimensional, complex, scattering vectors denoted by $\mathbf{k}_1$ and $\mathbf{k}_2$, respectively. Using the outer product formed from the scattering vectors $\mathbf{k}_1$ and $\mathbf{k}_2$, corresponding to each SAR image, it is possible to define the 6 by 6 complex, Hermitian, positive semidefinite matrix $[C_6]$. See section 2.4 for definitions.

As it is defined in Eq. (2.192) on page 49, the 6 by 6 complex matrix $[C_6]$ can be divided into four additional 3 by 3 complex matrices. The two matrices located at the diagonal of $[C_6]$, termed $[C_{11}]$ and $[C_{22}]$, correspond to the polarimetric covariance matrices of each one of the fully polarimetric datasets. Consequently, the corresponding sample covariance matrices $[Z_{11}]$ and $[Z_{22}]$ are completely characterized by the noise model given in Eq. (5.106). The off-diagonal matrix of $[C_6]$, which is denoted by $[\Gamma_{12}]$, contains additionally interferometric information as it has components acquired from different spatial positions. This matrix is defined as

$$[\Gamma_{12}] = E\left\{\mathbf{k}_1\mathbf{k}_2^{*T}\right\} = \begin{bmatrix} E\{S_{hh_1}S_{hh_2}^*\} & \sqrt{2}E\{S_{hh_1}S_{hv_2}^*\} & E\{S_{hh_1}S_{vv_2}^*\} \\ \sqrt{2}E\{S_{hv_1}S_{hh_2}^*\} & 2E\{S_{hv_1}S_{hv_2}^*\} & \sqrt{2}E\{S_{hv_1}S_{vv_2}^*\} \\ E\{S_{vv_1}S_{hh_2}^*\} & \sqrt{2}E\{S_{vv_1}S_{hv_2}^*\} & E\{S_{vv_1}S_{vv_2}^*\} \end{bmatrix} \tag{5.111}$$

where ^{*T} indicates transpose conjugate and $E\{\cdot\}$ is the expectation operator. Its corresponding single-look matrix, defined as

$$[Z_{12}] = \mathbf{k}_1\mathbf{k}_2^{*T} = \begin{bmatrix} S_{hh_1}S_{hh_2}^* & \sqrt{2}S_{hh_1}S_{hv_2}^* & S_{hh_1}S_{vv_2}^* \\ \sqrt{2}S_{hv_1}S_{hh_2}^* & 2S_{hv_1}S_{hv_2}^* & \sqrt{2}S_{hv_1}S_{vv_2}^* \\ S_{vv_1}S_{hh_2}^* & \sqrt{2}S_{vv_1}S_{hv_2}^* & S_{vv_1}S_{vv_2}^* \end{bmatrix} \tag{5.112}$$

is composed by Hermitian product pairs of polarimetric components acquired at the two spatial locations. The extended scatterer vector, defined as $[\mathbf{k}_1, \mathbf{k}_2]^T$, is statistically described by a multivariate, zero-mean, complex, Gaussian pdf, $\mathcal{N}(\mathbf{0}, [C_6])$. Consequently, the 6 by 6 complex single-look covariance matrix $[Z_6]$ is described by a complex Wishart pdf, $\mathcal{W}([C_6], 1)$. As a result of these definitions, it can be concluded

that the different elements of the single-look matrix $[Z_{12}]$ are described by the same distributions as the elements of the matrices $[Z_{11}]$ and $[Z_{22}]$. Consequently, the entries of $[Z_{12}]$ are characterized by the same speckle noise model as the elements of $[Z_{11}]$ and $[Z_{22}]$, Eq. (5.95). Finally, the vectorial speckle noise model for the extended sample covariance matrix $[Z_6]$ is obtained as a simple extension of the model presented in Eq. (5.106), taking into account the larger dimensionality of the problem in the case of PolInSAR data.

From a strictly statistical point of view, all the elements of the covariance matrix $[C_6]$ are characterized by the speckle noise model given by Eq. (5.95). Hence, the final nature of speckle noise for each element depends on the value of the complex correlation coefficient between the pair of SAR images from which the Hermitian product is constructed. The basic difference between PolSAR and PolInSAR data is the introduction of interferometric information. This new information will affect the correlation coefficient between the pair of SAR images producing, therefore, a change over the final speckle noise nature. On the other hand, the variation of the covariance value $|\rho|$ will affect the balance between the multiplicative and the additive speckle noise terms. On the other hand, as the phase difference ϕ_x is also changed due to the interferometric information, it will have an effect over the final speckle noise nature. In the following, it will be shown that the phase information acquires a key importance concerning the speckle noise nature of the real and imaginary parts of the Hermitian product for a pair of SAR images.

In Section 5.5.2, the Hermitian product speckle noise model has been validated with a L-band, fully polarimetric dataset over the area of Oberpfaffenhofen, acquired with the E-SAR system. This dataset is also a PolInSAR dataset, in which the second PolSAR dataset was acquired in a repeat-pass interferometric configuration, with a space baseline of 10 m approximately and a temporal difference of 10 min. As a result of the short time between both acquisitions, temporal decorrelation effects can be neglected. In this case, as done previously, only one element of the matrix $[\Gamma_{12}]$ will be analyzed, extending the results to the complete matrix. In this case, the term $S_{hh_1}S^*_{vv_2}$ is considered. Fig. 5.21 depicts the amplitude and the phase of the complex correlation coefficient between the SAR images S_{hh_1} and S_{vv_2}.

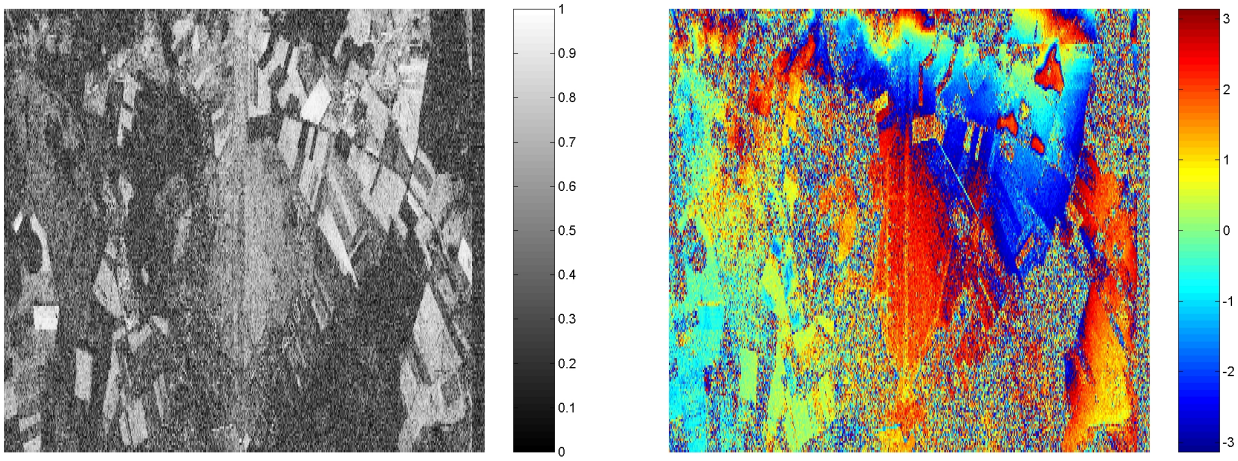

(a) (b)

Figure 5.21: Oberpfaffenhofen test site. Complex correlation coefficient ρ corresponding to the extended covariance matrix element $S_{hh_1}S^*_{vv_2}$. (a) Amplitude $|\rho|$. (b) Phase ϕ_x rad.

If one compares Fig. 5.21 with the corresponding to the polarimetric term $S_{hh_1}S^*_{vv_1}$, Fig. 5.16, it can be noticed that the coherence value presents only minor differences between both cases. Consequently, the effect of the variation of $|\rho|$ between both Hermitian products will not have too much effect over the final nature of speckle noise. On the contrary, if phases are compared, noticeable differences can be noticed due to the terrain's relief. As a result, the main changes on the final speckle noise nature, in the case of the elements $S_{hh_1}S^*_{vv_1}$ and $S_{hh_1}S^*_{vv_2}$, are induced by the differences on the corresponding phases ϕ_x. Fig. 5.23 presents the mean versus standard deviation scatter diagrams corresponding to

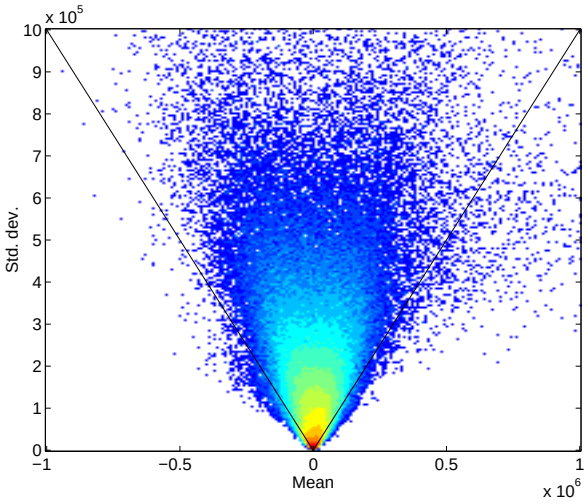

Figure 5.22: Global scatter diagram for $\Re\{S_{hh_1}S^*_{vv_2}\}$ in the case of the Oberpfaffenhofen test site.

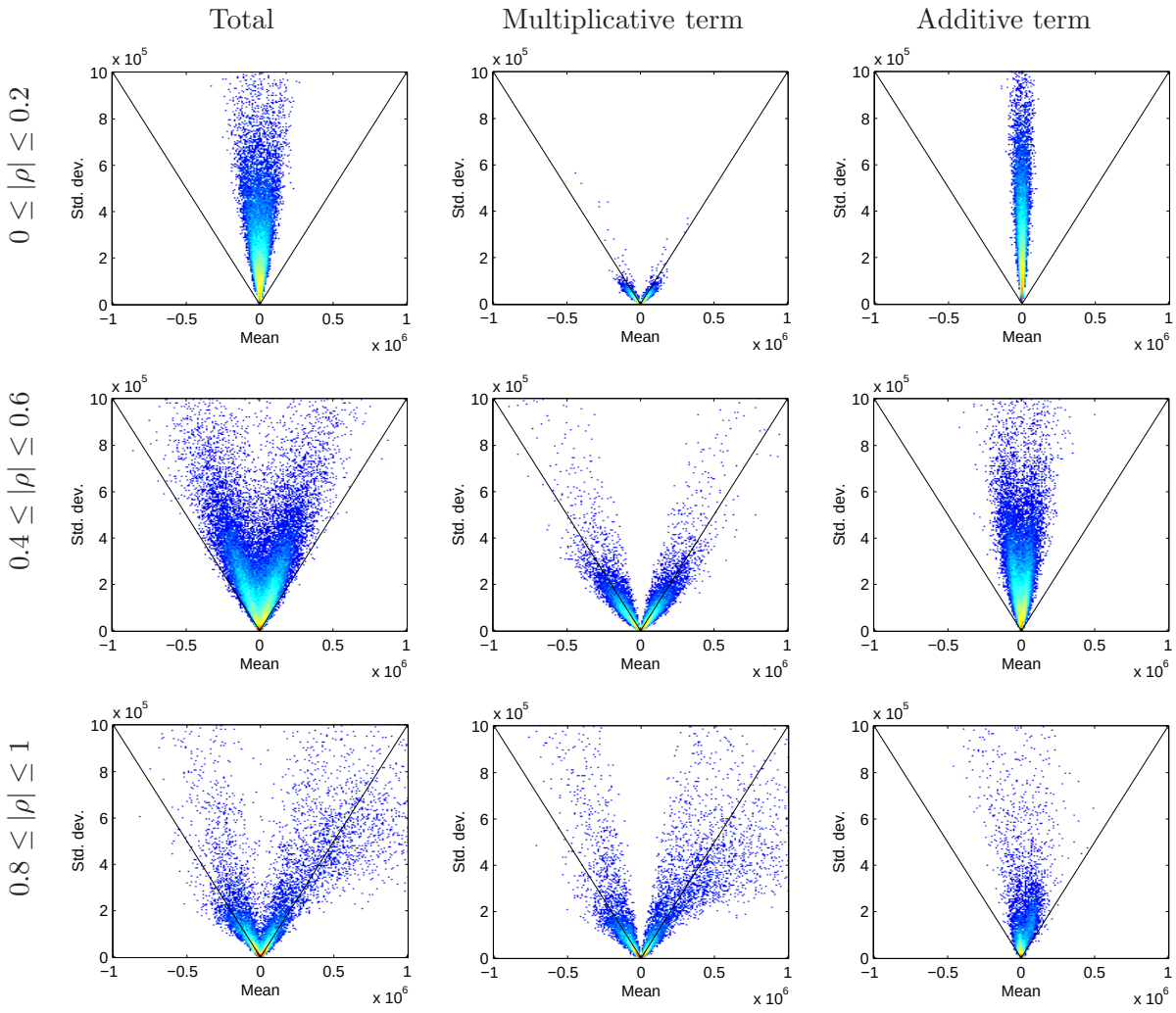

Figure 5.23: Scatter diagrams for $\Re\{S_{hh_1}S^*_{vv_2}\}$ in the case of the Oberfapfenhoffen test site.

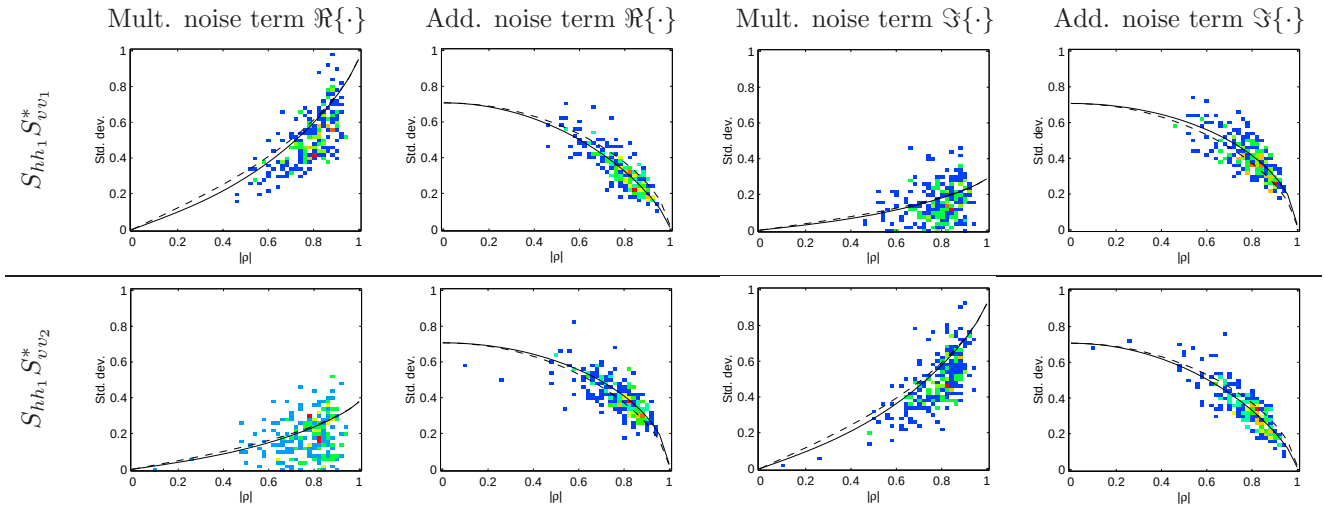

Figure 5.24: Standard deviations for the Hermitian product multiplicative and additive terms in the case of $S_{hh_1}S^*_{vv_1}$, a polarimetric covariance matrix term, and $S_{hh_1}S^*_{vv_2}$, a polarimetric interferometric covariance matrix term.

$\Re\{S_{hh_1}S^*_{vv_2}\}$, as well as the diagrams corresponding the multiplicative and the additive terms. As it was shown for PolSAR data, in the case of the real and imaginary parts of the Hermitian product for PolInSAR data, speckle noise is dominated by a multiplicative behavior for high coherences while it is almost additive for low ones.

But, if one compares Fig. 5.18 with Fig. 5.23 it can be observed that in the former case, all the scatter diagrams, specially those of the multiplicative component, are clearly biased to the right part of the diagram since the difference phase is basically centered in $\phi_x = 0$ rad. In the PolInSAR data, as it can be observed in Fig. 5.21, the phase ϕ_x is more heterogeneous as a consequence of the topographic component. This fact produces the scatter diagrams to be more centered on the plots. This effect is clearly visible for the multiplicative term dispersion diagrams since in the case of $\Re\{S_{hh_1}S^*_{vv_2}\}$ they populate the positive and the negative branches of the scatter diagrams.

The main conclusion at this point is that for those cases in which the Hermitian product contains interferometric information, the phase difference ϕ_x determines clearly, despite in an indirect way, the final nature of speckle noise. Therefore, it can be affirmed that the final nature of speckle noise, for the real and imaginary parts of those Hermitian products containing interferometric information, is determined by the terrain's topography and the scatterer's vertical structure. In order to test this fact, a common area has been selected from the SAR images $S_{hh_1}S^*_{vv_1}$ and $S_{hh_1}S^*_{vv_2}$. The selected region corresponds to a flat surface located in the upper left-hand corner of the Oberpfaffenhofen test site. The selected area corresponding to the product $S_{hh_1}S^*_{vv_1}$ has a complex coherence equal to $0.779\exp(j0.290)$, whereas the corresponding to $S_{hh_1}S^*_{vv_2}$ has a complex coherence equal to $0.770\exp(j1.189)$. Fig. 5.24 presents the standard deviation values for the multiplicative and the additive terms of the Hermitian products $S_{hh_1}S^*_{vv_1}$ and $S_{hh_1}S^*_{vv_2}$. As it can be observed in Fig. 5.24, for the Hermitian product $S_{hh_1}S^*_{vv_1}$, the real part is basically dominated, in terms of standard deviation, by a multiplicative noise whereas for the imaginary part, speckle noise is dominated by and additive nature. This situation changes if $S_{hh_1}S^*_{vv_2}$ is considered. As observed in Fig. 5.24, here the real part is dominated by the additive noise component and the imaginary is dominated by the multiplicative speckle noise term. Considering Eq. (2.124) on page 33, the coherences for the Hermitian products can be divided as

$$|\rho_{hh_1vv_1}| = |\rho_{pol}| \tag{5.113}$$

$$|\rho_{hh_1vv_2}| = |\rho_{pol}||\rho_{int}| = |\rho_{pol}|\,|\rho_{SNR}|\,|\rho_{temporal}|\,|\rho_{range}|\,|\rho_{volume}|. \tag{5.114}$$

In Eq. (5.114), $|\rho_{temporal}|$ can be considered to be equal to one due to the short delay between both acquisitions. Equally, $|\rho_{SNR}|$ can be assumed to be also to one since the influence of $|\rho_{SNR}|$ is restricted to areas characterized by a low backscattering behavior, which is not the case. The critical baseline at L-band for the E-SAR system equals approximately 300m. Since the interferometric baseline in this case represents a 3% of the critical baseline, $|\rho_{range}|$ can be considered equal to the unity. Since in both cases the coherence is equal to 0.77, it can be deduced that $|\rho_{volume}|$ is also equal to 1 (see Section 2.2.4 for additional details) confirming the fact that the selected area corresponds basically to a flat, bare area. Since in this case, phase variation is basically determined by the topography-induced phase, it demonstrates that the final nature of speckle noise, for those Hermitian products containing interferometric information, depends on the terrain's topography.

5.7 Multifrequency SAR Speckle Noise Model

As it has been mentioned in Section 5.5.3, a SAR sensor can acquire data at different frequencies. Consequently, the properties of the SAR data will depend on the frequency, affecting at the same time the correlation structure of multidimensional SAR data. The final result of this variation is that the speckle noise nature for the different Hermitian products of pair of SAR images will vary for the different frequencies. In this case, the variation of the speckle noise behavior is linked to the different response of a given scatterer to the different frequencies. Additionally, a change on the system's central frequency also implies, most of the times, a variation on some parameters of the SAR system itself. Among them, one of the most important is the variation on the system's bandwidth B. This parameter is crucial since the dimensions of the resolution cell, and in particular the range resolution, depend on it. Basically, the larger the bandwidth, the smaller the range resolution, see Eq. (2.1) on page 10. This fact has important consequences on the Hermitian product speckle noise model, since, the validity of the Gaussian scattering assumption, in which the noise model is based, depends at the same time on the assumption to have a sufficient number of scatterers within the resolution cell. This fact allows to assume distributed scatterers to be described by a zero-mean, complex Gaussian distribution. Consequently, the smaller the resolution cell dimensions, the most unprovable the assumption of Gaussian scattering model for scattered signals. In the following, the speckle noise model proposed for the Hermitian product of SAR images, Eq. (5.95) will be tested with SAR images acquired at different frequencies. The model is specifically tested over P-, L-, C- and X-band datasets. The first three datasets correspond to fully polarimetric datasets acquired on the same area, whereas the fourth one corresponds to an interferometric dataset of a different region. The Hermitian product speckle noise model is tested in the case of X-band over an InSAR dataset since a PolSAR dataset was non available at this band.

The P-, L-, and C-band data correspond to fully polarimetric datasets acquired with the AIRSAR system [16, 17, 18], operated by NASA, over the area of Les Landes, located on the South-West region of France. The SAR images correspond to a pine forest. The X-band data correspond, on the contrary, to an InSAR dataset acquired with the E-SAR system [186], operated by DLR in a single-pass interferometric configuration with an approximate baseline of 1.6 m, on the area of Oberpfaffenhofen, located on the West of the German city of Munich. In all the cases, the noise model is tested over an homogeneous region. In the case of the P-, L-, and C-band datasets, the model is tested over the same area in order to investigate

Frequency band	P (0.45 GHz)	L (1.26 GHz)	C (5.31 GHz)	X (9.6 GHz)
Sensor	AIRSAR	AIRSAR	AIRSAR	E-SAR
Range sp. resolution	7.5 m	3.75 m	1.875 m	2.2 m
Azimuth sp. resolution	1 m	1 m	1 m	1.8 m
Hermitian product	$S_{hh_1}S^*_{vv_1}$	$S_{hh_1}S^*_{vv_1}$	$S_{hh_1}S^*_{vv_1}$	$S_{vv_1}S^*_{vv_2}$
ρ	$0.737\exp(j0.179)$	$0.671\exp(j0.017)$	$0.458\exp(j0.025)$	$0.871\exp(-j0.648)$

Table 5.3: System and data parameters.

$\Re\{S_{hh_1}S^*_{vv_1}\}_P$	a_0	a_1	s	r
Mean mult.	0.004	0.987	0.012	0.990
Std. mult.	-0.026	0.997	0.078	0.774
Mean add.	0.008	0.960	0.012	0.675
Std. add.	0.022	0.929	0.048	0.820
C_{12}	-0.004	0.995	0.322	0.104

(a)

$\Re\{S_{hh_1}S^*_{vv_1}\}_L$	a_0	a_1	s	r
Mean mult.	0.003	0.985	0.012	0.990
Std. mult.	0.033	0.865	0.067	0.813
Mean add.	-0.021	1.153	0.013	0.682
Std. add.	-0.067	1.104	0.052	0.854
C_{12}	0.042	0.636	0.325	0.106

(b)

$\Re\{S_{hh_1}S^*_{vv_1}\}_C$	a_0	a_1	s	r
Mean mult.	0.001	0.992	0.012	0.985
Std. mult.	0.005	0.930	0.036	0.865
Mean add.	-0.002	1.034	0.012	0.939
Std. add.	-0.128	1.207	0.075	0.740
C_{12}	0.008	0.817	0.030	0.726

(c)

$\Re\{S_{vv_1}S^*_{vv_2}\}_X$	a_0	a_1	s	r
Mean mult.	0.006	0.986	0.007	0.997
Std. mult.	-0.057	1.164	0.156	0.664
Mean add.	0.006	0.950	0.007	0.960
Std. add.	-0.041	1.120	0.057	0.860
C_{12}	1.233	-0.256	3.062	0

(d)

Table 5.4: Multifrequency least squares regression analysis test results.

possible variations concerning the speckle noise model validity which depend on frequency. The model is also tested over an homogeneous area in the case of the X-band dataset. Table 5.3 presents a summary of the relevant system parameters for each frequency as well as the complex coherence corresponding to the four selected areas.

Equally, as it has been performed previously in this chapter, the validity of the noise model is quantitatively measured by means of a least squares regression analysis between the theoretical values of the different statistical parameters of the noise model components, as defined by Eq. (5.109), and the values estimated from real data employing the usual sample estimators over 7 by 7 pixel, non-overlapped, windows. The results of these analyses are given in Table 5.4. In this case, only the real parts of the Hermitian products are presented, since the results corresponding to the imaginary parts display the same information. As it can be observed in Table 5.4, the least squares regression analysis show the same level of agreement for the four frequencies. The interpretation of the different parameters of Table 5.4 can be found in Appendix D. The worst agreement is always obtained for the correlation parameter $\mathcal{C}_{12}$ as a consequence of the insufficient number of samples to estimate it. On the other hand, the best agreement between theory and data corresponds to the mean values of the multiplicative terms, which has been demonstrated to contain the major part of the signal to recover. The regression analysis corresponding to the standard deviation values have been performed with respect to the approximated theoretical values.

The main conclusion which can be extracted from the previous analysis is that the proposed speckle noise model for the Hermitian product of a pair of SAR images can be considered valid for a wide frequency range. Consequently, this validation allows to extend the Hermitian product speckle noise model to describe the Hermitian product of a pair of SAR images acquired at different frequencies.

As stated, multidimensional SAR imagery is important since it allows to increase the number of estimable parameters, concerning a given scatterer, from measured data. It has been shown recently, that multifrequency SAR systems can be also employed to retrieve scatterer information [181, 187]. The usefulness of this technique, for distributed scatterers, is based on the fact that the scattering from a given element changes only slightly with frequency, while the entire scatterer decorrelates faster. This is due to the fact that frequency decorrelation depends on changes in the relative positions between scatterers (phase changes) and not on the scatterers themselves. Let a radar system operating in a central frequency f_0 with a bandwidth B_w. This bandwidth accounts for a shift on the central frequency f_0, which is different from the system bandwidth B accounting for the pulse bandwidth. If the bandwidth B_w is a small fraction of the central frequency f_0, the backscattering coefficient will be approximately independent of frequency

$$E\{|S_f|^2\} \simeq E\{|S_{f_0}|^2\} \tag{5.115}$$

where S_f denotes a complex SAR image acquired at the central frequency f. Thus, the backscattered

process S_f becomes a stationary process and its covariance only depends on the frequency shift $\Delta f = f_2 - f_1$

$$\mathcal{C}_{f_1,f_2} = E\{S_{f_2} S_{f_1}^*\} = \mathcal{C}(f_2 - f_1) \tag{5.116}$$

where $\mathcal{C}$ denotes the statistical covariance. The frequency correlation function (FCF) is defined as the normalized covariance function, whose amplitude and phase are [181, 187]

$$R(\Delta f) = \left| \frac{\mathcal{C}(\Delta f)}{\mathcal{C}(0)} \right| \tag{5.117}$$

$$\Phi(\Delta f) = \arg\left(\frac{\mathcal{C}(\Delta f)}{\mathcal{C}(0)} \right). \tag{5.118}$$

Considering these definitions, the proposed speckle noise model for the Hermitian product introduced by Eq. (5.95) can be extended to the product of two SAR images acquired at different frequencies S_{f_1} and S_{f_2} as follows [188]

$$S_{f_2} S_{f_1}^* = \psi N_c \overline{z}_n n_m e^{j\Phi(\Delta f)} + \psi(R(\Delta f) - N_c \overline{z}_n) e^{j\Phi(\Delta f)} + \psi(n_{ar} + j n_{ai}). \tag{5.119}$$

The different parameters have to be redefined in this case. Inside the bandwidth B_w, the average power has the expression $\psi = E\{|S_{f_0}|^2\}$, where Eq. (5.115) has been used. As it has been demonstrated, N_c is a function of the coherence $|\rho|$, but in this case it is a function of $R(\Delta f)$. Equally, $\overline{z}_n$ depends on $R(\Delta f)$ instead of $|\rho|$. Finally, the additive noise terms n_{ar} and n_{ai} have a variance value where the parameter $|\rho|$ has to be interchanged by $R(\Delta f)$, see Eq. (5.92).

5.8 Summary

Within this chapter, and according to the results obtained in Chapter 4, a novel multidimensional speckle noise model has been obtained and validated. This new speckle model has been derived specially for multidimensional SAR data, and polarimetric SAR data in particular.

Multidimensional SAR data are considered under a covariance matrix representation. Within the first part of this chapter, the convenience of this representation is justified in two ways. On the one hand, the covariance matrix characterizes completely multidimensional SAR data under the Gaussian scattering assumption. On the other hand, since all the covariance matrix entries consist in a complex Hermitian product of two SAR images, the complete speckle model for the covariance matrix can be obtained by extending the Hermitian product speckle noise model.

The second part of this chapter presents the obtention of the speckle noise model for the complex Hermitian product of a pair of SAR images. It is worth to mention that this model, and therefore, the multidimensional speckle noise model, is obtained on the basis of the interferometric phasor noise model, which is extended to consider the phase difference of a general Hermitian product. Given this result, and after a detailed study of the different probability density functions coming from the complex Wishart distribution, it is possible to obtain the complex Hermitian product speckle noise model. As a result, it is proved that the Hermitian product speckle noise results from the combination of two noise mechanisms: a multiplicative and an additive noise. This combination is determined by the complex correlation coefficient between the pair of SAR images which determine the Hermitian product. Consequently, this novel speckle model is able to describe noise effects in the diagonal and the off-diagonal covariance matrix elements. This speckle model represents an extension of the multiplicative noise model for the intensity of a SAR image. The covariance matrix speckle noise model is obtained by extending the Hermitian product model to all its elements. Therefore, the covariance speckle noise nature will depend on the multidimensional SAR data's structure. The most important issue is that this extension does not depend on the number of SAR images.

The last part of this chapter contains an extensive validation of the proposed noise model. In a first stage, the different expressions which characterize the noise model are validated by means of simulated SAR data. This analysis confirms also that the combination of the multiplicative and the additive speckle terms is inhomogeneous, producing the complex Hermitian product noise to be also inhomogeneous. The multidimensional speckle noise model is also validated quantitatively by means of real polarimetric and polarimetric interferometric SAR data acquired with the E-SAR sensor. The main conclusion which can be extracted from these analyses is the robustness of the proposed noise model. This robustness is due to the fact that the model is derived from the scattering theory, through the assumption of Gaussian scattering, and not from a process in which an equation is adjusted to experimental data. The multidimensional speckle noise model is finally validated in P-, L-, C- and X- bands, permitting to extend the model to consider noise effects between SAR images acquired at different frequencies.